TÉCNICO LISBOA

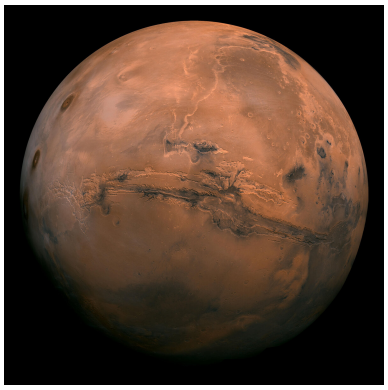

Rapid Crewed Missions to Mars: Impulsive Case

Filipe Alexandre da Costa Guerreiro Teixeira

Thesis to obtain the Master of Science Degree in

Aerospace Engineering

Supervisor: Prof. Paulo Jorge Soares Gil

Examination Committee

Chairperson: Prof. Paulo Jorge Coelho Ramalho Oliveira
Supervisor: Prof. Paulo Jorge Soares Gil
Member of the Committee: Prof. Orfeu Bertolami

January 2021

Dedicated to my family. . .

Acknowledgments

Queria agradecer ao Professor Paulo Gil pela sua orientação, paciência e disponibilidade em aconselhar esta etapa. Por todas as reuniões demoradas, discussões e feedback, que contribuíram largamente para um melhor trabalho.

Ao Professor Paulo Lopes, pela sua ajuda e partilha de conhecimento durante os meus primeiros anos académicos. Sobretudo pela sua boa disposição a ensinar, não só matemática mas também inúmeros outros tópicos através da sua experiência.

À Professora Maria Celeste Moniz, e aos seus métodos de ensino que, embora severos, contribuíram para a minha diligência.

Aos meus amigos, pelos bons tempos passados juntos.

E sobretudo, à minha Família. Por todo o suporte, por toda a orientação, por todas as lutas e reconciliações que se seguiram. Por toda a alegria, por toda a tristeza e por tudo entre as duas. Pelo amor incondicional e sacrifícios. Terão sempre um lugar especial no meu coração ...

Cover art: NASA, Jet Propulsion Lab, and California Institute of Technology, "Valles Marineris Hemisphere Enhanced," `https://mars.nasa.gov/resources/6453/valles-marineris-hemisphere-enhanced/`, July 2013. Retrieved 30 December 2020.

Resumo

Transferências de energia mínima têm, tipicamente, um tempo de transferência (só ida) de cerca de 259 d. Adicionalmente, uma estadia de cerca de 453 d é necessária para esperar por condições ótimas de retorno. Tempos longos aumentam o risco devido à radiação e a ambientes de gravidade reduzida. Estes podem ser reduzidos indo mais rápido, mas levam a penalidades na massa. Uma vez que massa e tempo são indicadores de custo e risco, respetivamente, viagens rápidas têm riscos menores, mas custos maiores.

Para verificar o impacto de várias escolhas na massa geral, os elementos requeridos para cada arquitetura de missão foram identificados e a sua massa estimada. Sistemas de propulsão representativos foram selecionados, para sistemas atuais e para futuros. Para estimar a massa de propelente, a equação do foguete foi modificada para incluir perdas por gravidade e o descarte de tanques vazios durante manobras. Esta inclusão levou a novos efeitos, não englobados pela equação tradicional, como a existência de um tempo total mínimo para a viagem.

Os resultados obtidos sugerem que missões rápidas podem não ser ainda atingíveis com massa razoável. Porém, são encorajadores para o futuro próximo. Como comparação, a Design Reference Architecture 5.0, a referência na exploração tripulada a Marte, indica uma massa inicial em órbita baixa de 849 t para um tempo de viagem total de 916 d. Para a mesma massa, uma duração de 200 d pode ser atingida com um impulso específico de 1 000 s e um rácio propulsão-peso de 75.

Palavras-chave: missões espaciais tripuladas, Marte, transferências rápidas, planeamento de missões espaciais

Abstract

Traditional minimum-energy transfers have a long transfer time (one leg) of about 259 d. Additionally, a stay of about 453 d is required to wait for the optimal return conditions. Such long times increase the risks posed by radiation and reduced gravity environments. These can be reduced by going faster, but lead to mass penalties. Since mass and time are proxies for cost and risk, respectively, rapid trips have lower risks but higher costs.

In order to assess the impact of several choices in the overall mass, required elements for each mission architecture were identified and its mass estimated. Representative propulsion systems were selected, for actual and for future systems. For propellant mass estimations, the rocket equation was modified in order to include gravity losses and the disposal of empty tanks during manoeuvres. The former lead to new effects, unperceived by the traditional equation, such as the existence of a minimum total trip time.

Obtained results suggest that rapid missions may not yet be achievable with reasonable mass. However, they are encouraging for the near future. As a comparison, the Design Reference Architecture 5.0, the benchmark in crewed Mars exploration, states an Initial Mass in Low Earth Orbit of 849 t for a total trip time of 916 d. For the same mass, a duration of 200 d can be achieved with a specific impulse of 1 000 s and a thrust-to-weight ratio of 75.

Keywords: crewed space missions, Mars, rapid transfers, space mission design

Contents

List of Tables

List of Figures

Nomenclature

c	A constant in a regression
d	Mission duration, d
g	Gravitational acceleration at Earth's surface, $\mathrm{m/s^2}$
I_{SP}	Specific impulse, s
K	Ratio between propellant tank mass and propellant mass
m	Mass, kg
$m_{\text{non-TPS}}$	Mass excluding the Thermal Protection System (TPS), kg
$m_{\text{structure}}$	Structural mass of the Transit Habitat (THAB), kg
m_{TPS}	Mass of the Thermal Protection System (TPS), kg
N	Number of rocket stages
N_{crew}	Number of crewmembers
Q	Total heat load, $\mathrm{J/m^2}$
r	Distance to the primary when executing a propulsive manoeuvre, m
T	Thrust, N
t_{burn}	Propulsive manoeuvre duration, s
V	Volume of the Transit Habitat (THAB), $\mathrm{m^3}$
W	Weight of the propulsion system, N
Δv	Total change in velocity (including burn losses), $\mathrm{m/s}$
Δv_{ideal}	Change in velocity for the ideal impulsive manoeuvre, $\mathrm{m/s}$
Δv_{losses}	Additional change in velocity to compensate burn losses, $\mathrm{m/s}$
ϵ	Structural ratio
μ	Gravitational parameter of the primary, $\mathrm{m^3/s^2}$

ϖ	Payload ratio
χ	Thermal Protection System (TPS) mass fraction

Subscripts

$*$	Payload
0	Initial
f	Final
k	Index
p	Propellant
s	Structure

Glossary

ADCS Attitude Determination and Control System. xiii, 11

CDRA Carbon Dioxide Removal Assembly. xiii, 8, 9

CM Command Module. xv, 11

CRS Carbon Dioxide Reduction System. xiii, 9

DHCS Data Handling and Control System. xiii, 11, 12

DRA Design Reference Architecture. 2, 6, 12, 14, 25, 31, 39

ECLSS Environmental Control and Life Support System. xiii, 8, 11

EDL Entry, Descent and Landing. xiii, 5–7

EPS Electrical Power System. xiii, 11, 12

EVA Extravehicular Activity. xiii, 13

FSPS Fission Surface Power System. xiii, 5, 8

IAD Inflatable Atmospheric Decelerator. xiii, 5, 7

IMLEO Initial Mass in Low Earth Orbit. xv, xvi, 2, 3, 5, 7, 23, 25–33, 39, 40

ISRU In Situ Resource Utilisation. xiii, xiv, 2, 3, 5–8, 12–15, 30, 32, 39

ISS International Space Station. xiii, xv, 6, 8–11

LEO Low Earth Orbit. 18

LM Lunar Module. xv, 11

MAV Mars Ascent Vehicle. xiii, 6, 12–14

MDM Mars Descent Module. xiii, 6, 12, 13

MOI Mars Orbit Insertion. xiii, 2, 5, 7

OGS Oxygen Generation System. xiii, 9

RCS Reaction Control System. xiii, 13

SHAB Surface Habitat. xiii, 6, 12–14

SPS Solar Power System. xiii, 5, 8

TCS Thermal Control System. xiii, 11

THAB Transit Habitat. xiii, xvii, 6, 9, 10, 12, 13, 18, 19

TPS Thermal Protection System. xiv, xv, xvii, xviii, 7, 8, 15, 16, 39

TRL Technology Readiness Level. 2, 22, 23

UPA Urine Processor Assembly. xiii, 9

WPA Water Processor Assembly. xiii, 9

WRS Water Recovery System. xiii, 9

Chapter 1

Introduction

1.1 Objectives and Motivation

This work is a preliminary assessment of the feasibility of rapid crewed round-trip missions to Mars with high-thrust propulsion. By rapid, it is meant a total travel time up to a few months. Shorter times lessen the risks to the crew but incur in mass penalties due to extra propellant needs. By selecting architectures focused on the essentials, the trade-off may become favourable and competitive with longer missions.

1.2 Challenges of Crewed Missions to Mars

When considering interplanetary travels to Mars, minimum-energy transfers tend to be chosen. Although this is a measure to reduce the mission mass, the travel time is largely compromised. For one-way missions, the outbound travel takes around $259\,\mathrm{d}$ [1]. For round trips (e.g. sample returns and most crewed missions), a stay of about $453\,\mathrm{d}$ is also required to wait for the optimal return conditions [1].

Such extensive times imply a long exposure to dangers such as radiation and reduced gravity, both present during the travel and the stay. Galactic cosmic radiation is the long-term predominant form of radiation [2], while solar particle events are sporadic and well correlated with the Sun's period of most intense activity [2]. As for reduced gravity, significant, long-term physiological changes are induced: blood loss, muscle atrophies, bone demineralisation, fatigue and performance loss [3]. These are more severe during the interplanetary travel, but should present during the stay as well.

Rapid missions mitigate these adversities by decreasing the exposure time. However, much higher changes in velocity are required in order to achieve significant reductions [4]. Since mission mass and duration can be defined as a proxy to cost and risk, respectively, minimum-energy transfers minimise the mission cost by accepting higher risks while rapid missions minimise the risk by accepting higher costs.

1.3 Literature Review

Several proposals have been made in an effort to assess costs and risks of different options for crewed missions to Mars. Of particular importance is the Design Reference Architecture (DRA) 5.0 [5], which constitutes a benchmark for the community. Nonetheless, the relevance of some architectural choices are questionable [6]. Of these, crew size is perhaps the most important due to its large impact across most systems [6, 7].

In order to decrease risk, a split scenario can be used, in which the mission is divided into cargo and crewed components [5]. Although it might be debatable whether or not this is effective in certain cases [8], it is vital in the context of rapid trips since it also significantly reduces the mass of the mission. The crew can fly in a faster, safer trajectory while the cargo can be sent on an efficient minimal-energy transfer.

Aerocapture can also be employed in order to decrease the required mass, by reducing, or even eliminating, the propellant needed for the Mars Orbit Insertion (MOI) [5]. However, the large payloads associated with human class missions may be problematic [9]. Furthermore, the high velocities inherent to rapid travels increase the complexity of the problem.

In Situ Resource Utilisation (ISRU) is yet another option to decrease the mission mass, which is typically considered for the production of Mars ascent propellant and life support consumables [5, 10, 11]. The technology still has a low Technology Readiness Level (TRL) [12], but it is estimated that $1\,\mathrm{kg}$ of Mars produced fuel reduces Initial Mass in Low Earth Orbit (IMLEO) by about $10\,\mathrm{kg}$ [11]. However, the larger benefit for rapid travels lies in the ISRU for the production of return propellant. Unfortunately, information regarding this topic has not been found.

More creative trajectories can also be utilised to lower the required velocity changes. One such alternative employs Venus flybys in either or both legs of the journey [13]. Despite allowing for faster travel times than minimum-energy transfers [13], these are not fast enough to be considered in the context of this work. Another alternative lies in cycler orbits, which maintain a constant movement between Earth and Mars through successive flybys at the planets [14]. In this case, the interplanetary spacecraft does not need to change its orbit, but a smaller spacecraft is needed to ferry the crew to and from each planet. Overall, there is a high initial set-up cost and long travel times [14], which make them more suited to long, sustained missions rather than short, isolated ones. For the same purpose, it has also been proposed to use a rotating tether system to launch and capture spacecrafts from each planet, which could reduce the transfer time to $94\,\mathrm{d}$ with aerobraking (or between $130\,\mathrm{d}$ to $160\,\mathrm{d}$ without it) [15]. The construction and deployment of such system carries its own set of problems, and does not seem to be neither in progress nor planned for the near future. Therefore, it was not considered further.

Rapid crewed missions to Mars have already been addressed and were found competitive with the DRA 5.0 [1, 4]. However, the focus was primarily on the design of the interplanetary portion, and did not delve as deep in the system engineering aspects. The complete mass analysis was performed only for a total travel time of $407\,\mathrm{d}$, with rough estimations for the cargo mission. Different propulsion systems were not investigated either. Another study focused on the comparison of four propulsion systems (including

future proposals) and reported difficulties in obtaining significant reductions for the total travel time [16]. Still, that conclusion was drawn in the absence of ISRU and aerocapture, and the parameters for the selected propulsion systems might have been overly conservative.

1.4 Overview

The developed work starts with a high-level analysis of possible mission scenarios. Architectural options are discussed and trimmed to a manageable size, based on the most promising ones. Then, mass and size of the required elements are estimated. The rocket equation is also adapted to include burn losses and the benefits of propellant tank staging.

Next, a brief review of current and advanced propulsion systems is performed and representative values for characteristic parameters are selected for high-thrust systems, compatible with the impulsive manoeuvre approximation.

Finally, Pareto fronts for IMLEO against total travel time are obtained and the results analysed in the context of rapid crewed missions to Mars.

Chapter 2

Mission Design

2.1 Architectural Choices

There are myriad ways of reaching Mars. Distinct features, such as ISRU or a different crew size, require different plans, each with its own corresponding mass. In order to analyse and compare these options, the required elements must be identified, pieced together into a coherent architecture and its mass estimated. Only then can the overall mass of each architecture be estimated and weighted against its benefits.

At each stage, there are multiple choices. Table 2.1 summarises the most prominent. From here, two

Choice	Possibilities					
Crew size [5, 7, 17, 18]	1	2	3	4	5	6
Cargo deployment [5, 8]	Pre-deployment				All-up	
MOI [5, 6, 19]	Direct		All-propulsive		Aerocapture	
EDL strategy [6]	All-propulsive			Rigid aeroshell		IAD
ISRU [5, 6, 11, 12]	None	Atmosphere-based		Atmosphere-based with regolith		
Surface power system [5]	SPS			FSPS		
Return strategy [20, 21]	Skip entry			All-propulsive		
Propulsion [16]	Impulsive thrust			Continuous thrust		

Table 2.1: Summary of key architectural options. Acronyms: Mars Orbit Insertion (MOI), Entry, Descent and Landing (EDL), Inflatable Atmospheric Decelerator (IAD), In Situ Resource Utilisation (ISRU), Solar Power System (SPS) and Fission Surface Power System (FSPS).

different approaches can be carried in order to select an architecture. An extensive one implies the computation of selected figures of merit across all possibilities. This can reveal less intuitive advantages but, at $2\,592$ different combinations, be very time consuming. Often, studies follow a baseline architecture, established on certain hypotheses, and conduct individual trades [22]. This was the method taken to trim the combinations to a manageable number[1] and allow a direct comparison between the survivors. IMLEO was chosen as the figure of merit due to its widespread use and consensus in being a well defined cost metric [22]. The focus of this work is then to assess the impact of the mission alternatives

[1] This merely removes trimmed architectures from the subsequent analyses but does not rule them out as viable options.

(specially the propulsion) in said metric. Where applicable, the best options were selected (according to the literature) and possible issues identified for further study.

Independently of the architecture, all missions must include a Transit Habitat (THAB) and the associated propulsion system, propellant and propellant tanks. The last are predicted to be numerous for rapid missions, and are discarded during the manoeuvres when empty. This is the bare minimum for an Apollo-like mission to Mars, with reduced exploration goals when compared to long-stay missions. Nonetheless, other elements may or may not be included depending on the specific architecture. In line with the DRA 5.0, the following elements were also incorporated: Mars Descent Module (MDM), Surface Habitat (SHAB), surface power system, Mars Ascent Vehicle (MAV) and re-entry capsule.

Generally, the mission can be divided into a crewed mission and two cargo missions, which Figs. 2.1 to 2.4 synthesise in a graphical manner. Cargo mission I carries elements that can be left in a parking

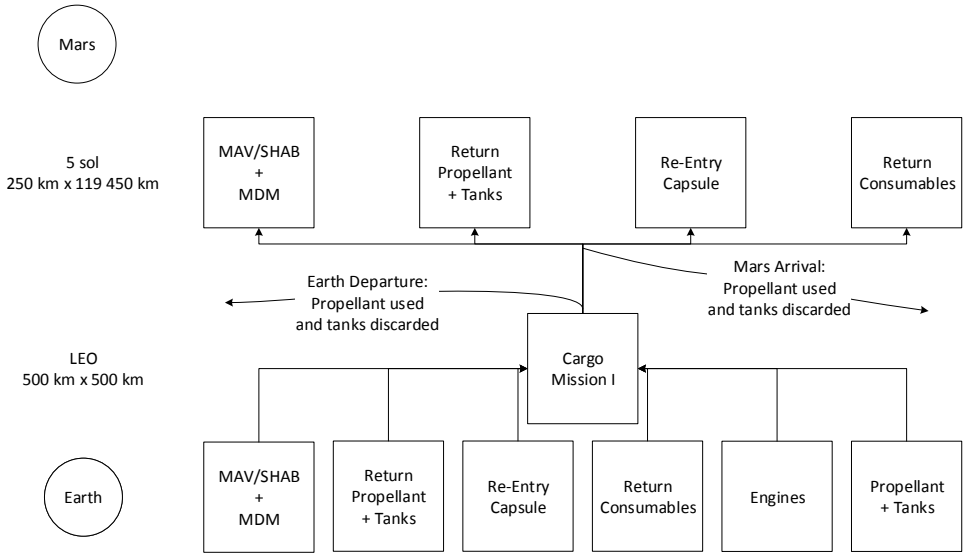

Figure 2.1: Bat diagram for cargo mission I. Acronyms: Mars Ascent Vehicle (MAV), Surface Habitat (SHAB), Mars Descent Module (MDM) and Low Earth Orbit (LEO).

orbit, while cargo mission II delivers onto the surface the elements required for the stay. The latter is done with the aid of MDMs. Elements division is summarised in Table 2.2. In every case, the crew departs in the THAB, which is put into a high-energy Mars parking orbit upon arrival. Return propellant tanks are then loaded from the cargo spacecraft into the THAB. Next, the crew descends to the surface, performs the required activities and ascends in the MAV when the stay is over. The MAV then carries the astronauts back to the THAB for the return journey. When approaching Earth, the crew shifts into the re-entry capsule and the THAB is discarded. Propulsive manoeuvres are used throughout except in this last stage, where it may not be needed (discussed further in Section 2.2.9).

Specifically, operations differ only in the descent and ascent portion of the mission. For architectures including ISRU, the MAV needs to be sent onto the surface in order to be fuelled. In this case, the SHAB is used by the crew for the descent. This is not required for architectures without ISRU, in which the SHAB can be sent to the surface and the MAV used for both descent and ascent.

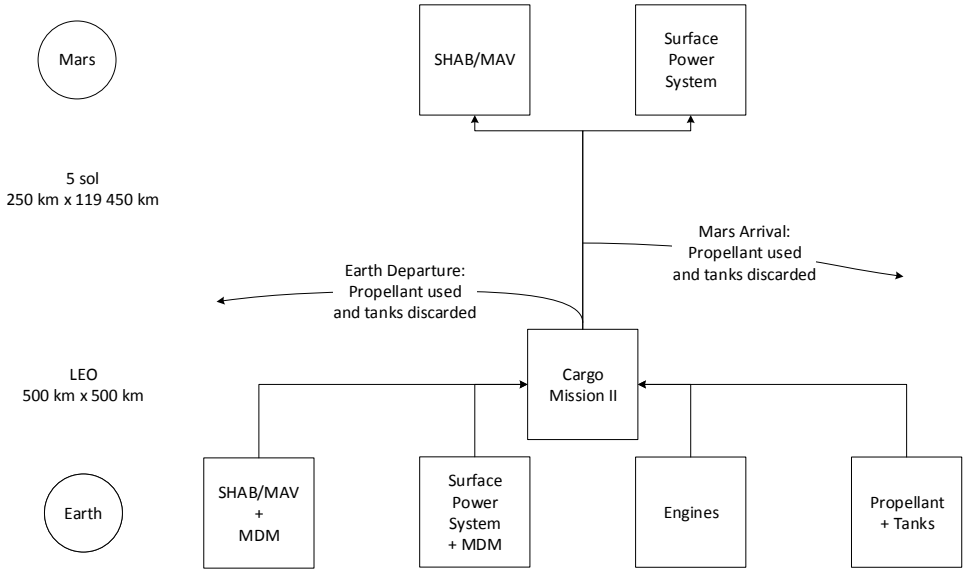

Figure 2.2: Bat diagram for cargo mission II. Acronyms: Mars Ascent Vehicle (MAV), Surface Habitat (SHAB), Mars Descent Module (MDM) and Low Earth Orbit (LEO).

Element	Mission
THAB	Crewed
MDM	Cargo II
SHAB	Cargo I or Cargo II
Surface power system	Cargo II
MAV	Cargo I or Cargo II
Return propellant	Cargo I
Re-entry capsule	Cargo I
Return consumables	Cargo I

Table 2.2: Elements and corresponding mission for the outbound portion of the travel. Acronyms: Transit Habitat (THAB), Mars Descent Module (MDM), Surface Habitat (SHAB) and Mars Ascent Vehicle (MAV).

A crew of two is the obvious choice to minimise mass [18]. This is not unprecedented, since some International Space Station (ISS) expeditions have featured only two members[2]. Crew size has a big impact in numerous subsystems, be it direct (e.g. life support system) or indirect (e.g. Entry, Descent and Landing (EDL) and aerocapture) [7]. Typical values range from three to six astronauts, selected in a top-down manner [5, 7, 17, 23], but can be as low as one [18]. It has been suggested that any crew should feature at least one member per each type of personnel: an engineer or technician, a geologist or biologist, and a doctor [7]. However, functions performed by a doctor can be bypassed for shorter missions. Unlike longer ones, the reduction in exposure to the risk environment decreases the value that a doctor might have.

Cargo was chosen to be pre-deployed in separate spacecrafts. Sending the crew in a fast trajectory is a measure to reduce exposure to space hazards. This comes at the expense of a large mass penalty

[2]Garcia, M., "Past Expeditions," `https://www.nasa.gov/mission_pages/station/expeditions/past.html`, February 2020. Retrieved 17 December 2020.

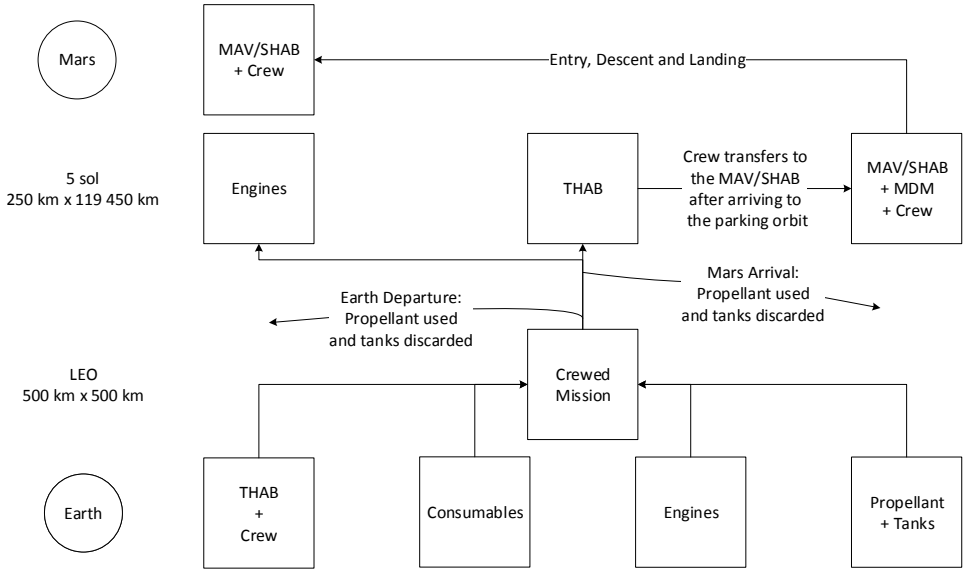

Figure 2.3: Bat diagram for the outbound portion of the crewed mission. Acronyms: Transit Habitat (THAB), Low Earth Orbit (LEO), Mars Ascent Vehicle (MAV), Surface Habitat (SHAB) and Mars Descent Module (MDM).

but the same requirement does not apply to the cargo, which can be sent in a low energy transfer at a prior date. Doing so leads to longer systems cumulative time but significantly reduces the total IMLEO [5].

Propulsive braking was selected as the method for MOI. Direct entry is not adequate for the fast mission concept. The associated velocities are large and Mars' atmosphere is thinner than Earth's. Aerocapture is usually an option to lower propellant mass, but it was not considered in this work because it poses serious challenges in this context. Namely, can the propulsion system stay attached during the manoeuvre, or is another system required for the return trip? Can solar panels be retracted during the manoeuvre? Can the Thermal Protection System (TPS) be re-utilised? Can aerocapture support the typically large payloads associated with crewed missions? Furthermore, aerocapture loses some of its value when applied to fast missions. For such large velocities, most of the braking would likely have to be done with propellant anyway. Aerocapture has huge difficulties that must be addressed in an in-depth study that lies outside the scope of this work.

For the EDL, a rigid aeroshell was chosen. All-propulsive solutions were not selected due to the large payload mass fractions expected [5]. As for Inflatable Atmospheric Decelerators (IADs), initial DRA 5.0 data was lacking in the desired range and extrapolations were too big to be considered acceptable [5]. A detailed EDL analysis was not performed, and the required values were taken from DRA 5.0 instead.

ISRU for Mars ascent propellant production was left open for comparison, and the three options available are summarised in Table 2.3. All the required elements can be produced on-site if water is retrieved from Martian regolith [11]. However, additional equipment is necessary in order to mine it. Besides, the operation of said equipment, like excavators and haulers, has unresolved significant challenges [5].

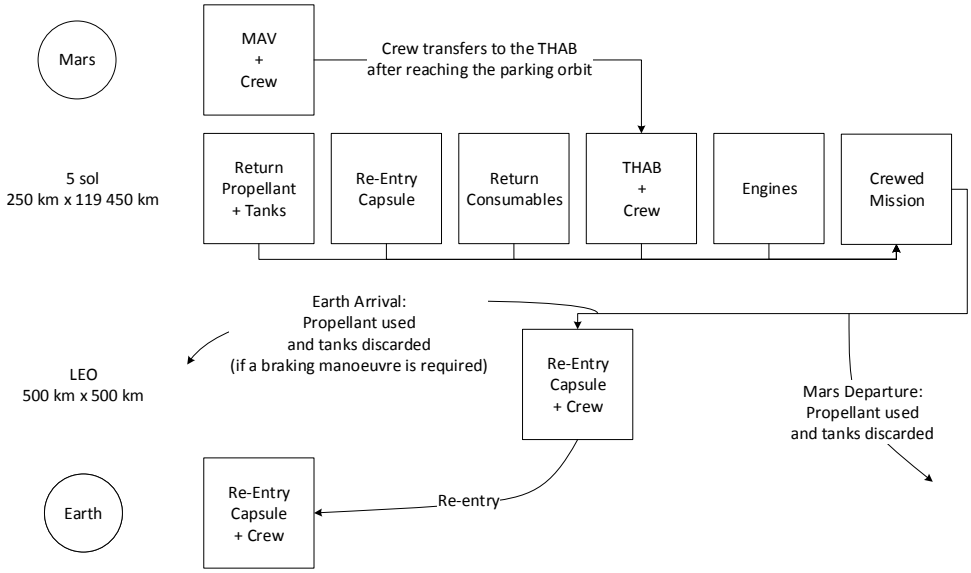

Figure 2.4: Bat diagram for the return portion of the crewed mission. Acronyms: Mars Ascent Vehicle (MAV), Transit Habitat (THAB) and Low Earth Orbit (LEO).

ISRU type	Product	Reagent	Source
None	O_2	–	Earth
	CH_4	–	Earth
Atmosphere-based	O_2	CO_2	Martian atmosphere
	CH_4	–	Earth
Atmosphere-based with regolith	O_2 and CH_4	CO_2	Martian atmosphere
		H_2O	Martian regolith

Table 2.3: ISRU types summary. Acronyms: In Situ Resource Utilisation (ISRU).

The surface power system decision is dependent on the ISRU strategy. For architectures employing ISRU, a Fission Surface Power System (FSPS) was chosen [5]. This allows a continuous operation of the ISRU plant while a Solar Power System (SPS) is limited to eight hours per day[3] and results in higher power needs [5]. Additionally, the former has a lower mass and it is easier to deploy autonomously [5]. Without ISRU both options are left open. The crew can deploy the solar arrays on arrival, eliminating the complexities associated with autonomous deployment. Lower power requirements [5] also reduce system mass making the solar option more competitive.

The preferred return strategy is the skip entry, which naturally encompasses direct entries (i.e. skip entries with zero skips). Direct entries are more easily controlled, but skipping in the atmosphere allows for cool-down periods which limit the amount of aerodynamic heating [21]. Historically, difficulties stemmed from computational limitations [21], but improvements in Earth approach navigation [24] have reduced this issue. A skip entry is also endorsed in the DRA 5.0 [20]. Nonetheless, some cases require some degree of propulsive braking in order to cope with the re-entry limits (either heat or maximum

[3]A large quantity of fuel cells reactants would be needed for continuous operations [5].

acceleration thresholds). Details regarding re-entry and TPS mass estimation can be found in Section 2.2.9.

Summarising, the considered options regarding the ISRU and the surface power system are listed in Table 2.4.

Option	ISRU	Surface power system
A	None	SPS
B	None	FSPS
C	Atmosphere-based	FSPS
D	Atmosphere-based with regolith	FSPS

Table 2.4: Considered ISRU and surface power system options. Acronyms: In Situ Resource Utilisation (ISRU), Solar Power System (SPS) and Fission Surface Power System (FSPS).

2.2 Mass Budget

2.2.1 Consumables

In order to estimate the mass of the consumables, a choice must be made between an open- and a closed-loop Environmental Control and Life Support System (ECLSS). For this end, Table 2.5 summarises the recycling systems available in the ISS along with their mass, consumables mass that would be saved should the system be implemented and number of days required for the system to be worth [25]. It can be seen that most systems require longer missions in order to be beneficial. The Carbon

System	System mass, kg	Spares* mass, kg	Total mass, kg	Mass use for a crew of two, kg/d	Break-even, d
OGS	676	399	1 075	3.36	319.9
CDRA	195	156	351	3.50	100.3
CRS	329	219	548	1.64	334.1
UPA + 31 %WPA†	742	366	1 108	2.88	384.7
69 %WPA‡	641	353	994	6.42	154.8
WRS§	1 383	719	2 102	9.30	226.0

* One set only.
† Urine processing system, requiring the UPA and 31 % of the WPA [25].
‡ Condensate and hygiene processing, comprised by 69 % of the WPA [25].
§ Composed by the UPA and WPA [25].

Table 2.5: Mass of consumables recycling systems, based on the ISS. Data retrieved from [25] and adapted for a crew of two. Acronyms: Oxygen Generation System (OGS), Carbon Dioxide Removal Assembly (CDRA), Carbon Dioxide Reduction System (CRS), Urine Processor Assembly (UPA), Water Processor Assembly (WPA) and Water Recovery System (WRS).

Dioxide Removal Assembly (CDRA) is the one with the lowest break-even value at around 100 d. This value sits towards the end of the range of interest, and calculations involved only one set of spares. It is not unusual to have more [25], which would further lower the benefit. Therefore, an open-loop ECLSS was preferred for this application.

Water requirements can be seen in Table 2.6. For the open-loop ECLSS, the corresponding con-

Purpose	Mass, $\mathrm{kg\,d^{-1}\,person^{-1}}$
Hydration	2.0
Food rehydration	0.5
Personal hygiene	0.4
Total	2.9

Table 2.6: Water mass per allocation per day and per person. Data retrieved from [26].

sumables are given in Table 2.7. Water and oxygen storage tank masses are considered separately in

Consumable	Mass, $\mathrm{kg\,d^{-1}\,person^{-1}}$
Food	2.39*
Water	2.90†
Oxygen	0.82‡
Lithium Hydroxide§	1.75‖
Total	7.86

* ISS value from 2017 (including packaging) retrieved from [27].
† Retrieved from Table 2.6.
‡ Nominal value retrieved from [27].
§ Needed for carbon dioxide removal [25].
‖ Retrieved from [25]. Includes the canister mass.

Table 2.7: Consumables mass per day and per person. Acronyms: International Space Station (ISS).

Table 2.8.

Consumable	Mass, kg per consumable kg	Mass, $\mathrm{kg\,d^{-1}\,person^{-1}}$
Oxygen	0.236	0.194
Water	6.136×10^{-3}	1.779×10^{-2}

Table 2.8: Mass of storage tanks. Data retrieved from [28].

Remaining consumables are divided based on usage frequency (one time or daily) and amount (one per crewmember or one for the whole crew). These are summarised in Table 2.9.

2.2.2 Mars Transit Habitat

At a high level, the THAB can be divided into structure, radiation shielding, accommodations and subsystems.

In order to estimate the structural mass, it is necessary to estimate the required habitable volume. To that end, the maximum mission duration was plotted against the minimum volume required per crewmember for a mission of such duration, in the case of several historical spacecraft (Fig. 2.5). It was necessary to include stations in order to provide data for longer missions. However, a regression including both Skylab and ISS, corresponding to the green full line in Fig. 2.5, did not capture the data

Consumable	Mass
One time, kg	182.500 0
One time per crewmember, kg	51.625 0
Daily, $\mathrm{kg\,d^{-1}}$	0.312 5
Daily per crewmember, $\mathrm{kg\,d^{-1}}$	1.813 3

Table 2.9: Other consumables including personal stowage, medical, hygiene and cleaning supplies. Data retrieved from [28].

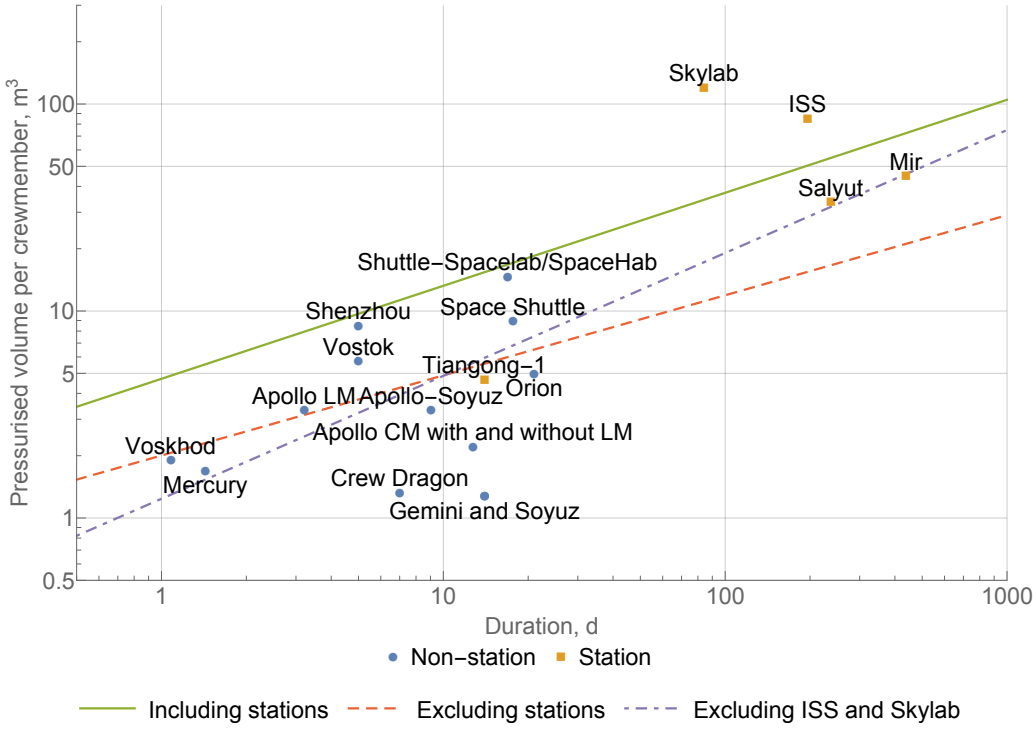

Figure 2.5: Correlation between pressurised volume per crewmember and duration. Blue dots and orange squares represent non-stations and stations, respectively. The green full line, red dashed line and purple dash-dotted line correspond to a regression including stations, a regression excluding stations and a regression excluding just the ISS and the Skylab, respectively. Acronyms: International Space Station (ISS), Lunar Module (LM) and Command Module (CM).

for lower mission times. Since Skylab was adapted from the upper stage of a Saturn Rocket[4], and ISS is a modular space station with collaboration from several different countries, it is likely they were not built with habitable volume in mind and were not considered further. The chosen fit was the purple dash-dotted line in Fig. 2.5, since it provides data for longer durations but does not forgo the data for shorter ones. The corresponding expression is given by

$$V/N_{\text{crew}} \approx 1.239 d^{0.594}, \tag{2.1}$$

where V is the volume of the THAB, N_{crew} is the number of crewmembers (two for this work) and d is the mission duration in days.

[4]Whiting, M., "Skylab: America's First Space Station," `https://www.nasa.gov/feature/skylab-america-s-first-space-station`, May 2018. Retrieved 17 December 2020.

A similar analysis was conducted to relate structural mass and volume. Since the habitat is a shell, structural mass is proportional to the surface area and scales with the two-thirds power of the volume [29]. A cylindrical shape was chosen over a conical shape since it lead to a lower mass for the same duration. Furthermore, conical shapes are prevalent in re-entry scenarios, which is not needed for the THAB. Using Eq. (2.1), the structure mass can then be given as a function of the duration by the expression

$$m_{\text{structure}} \approx 106.304 V^{2/3} \approx 122.606 \left(N_{\text{crew}} d^{0.594}\right)^{2/3}, \tag{2.2}$$

where $m_{\text{structure}}$ is the structural mass of the THAB.

For the radiation shielding, a side-wall density of $20\,\mathrm{g/cm^2}$ was considered to be enough [5]. The cylinder base and top do not require extra shielding, since there are usually other elements (propulsion system, for example) that already provide enough of it [28].

Accommodations were selected for short-term missions and focused on the essentials [28].

Subsystems mass and power are shown in Table 2.10. Apart from the consumables mass, an open-loop ECLSS still requires some basic equipments which contribute to the mass and power budget. Thermal Control System (TCS) mass and power is not significantly affected by crew size: comparison between crews of two and four members revealed differences below $50\,\mathrm{kg}$ and below $50\,\mathrm{W}$ in mass and power, respectively [28]. Thus, constant mass and power were assumed. Attitude Determination and Control System (ADCS) mass and power is independent of spacecraft size since the involved velocities are very small [28]. Fuel consumption is either negligible or accounted for in propulsion system margins, for the same reason [28]. The Data Handling and Control System (DHCS) achieves communications between Earth and the spacecraft [28]. Mass and power requirements do not change significantly for missions inside the inner solar system, despite being dependent on the exact trajectory [28]. Values were estimated from the Mars reconnaissance orbiter hardware [28]. The Electrical Power System (EPS) consists of solar panels capable of achieving Sun orientation, along with a storage and control unit [28].

Element	Mass, kg	Power, W
ECLSS [28]	1 207.0	2 294.6
TCS [28]	1 053	878
ADCS [28]	623	276
DHCS [28]	94.4	283
EPS	1 032.6*	–
Total	4 010.0	6 226.6

* Value calculated following the analysis provided in [28].

Table 2.10: Subsystems mass and power budget. Acronyms: Environmental Control and Life Support System (ECLSS), Thermal Control System (TCS), Attitude Determination and Control System (ADCS), Data Handling and Control System (DHCS) and Electrical Power System (EPS).

The THAB mass budget is summarised in Table 2.11.

Element	Mass, kg
Structure	$122.6 \left(N_{\text{crew}} d^{0.6}\right)^{2/3}$
Radiation shielding	$804.4 \left(N_{\text{crew}} d^{0.6}\right)^{2/3}$
Accommodations	670.9
Subsystems	4 010.0

Table 2.11: THAB mass budget. Acronyms: Transit Habitat (THAB).

2.2.3 Surface Habitat

The SHAB is designed for a smaller duration, but shares the same characteristics of the THAB. The exception is the EPS. Thus, the SHAB mass budget is very similar to the THAB, and is shown in Table 2.12. The SHAB power budget is the same, since the EPS does not contribute for it.

Element	Mass, kg
Structure	$122.6 \left(N_{\text{crew}} d^{0.6}\right)^{2/3}$
Radiation shielding	$804.4 \left(N_{\text{crew}} d^{0.6}\right)^{2/3}$
Accommodations	670.9
Subsystems	2 977.4

Table 2.12: SHAB mass budget. Acronyms: Surface Habitat (SHAB).

2.2.4 Crew and Samples

When estimating crew mass, an average of $82\,\text{kg}$ was used for each crewmember [27].

For samples, the total mass was assumed to be $239\,\text{kg}$ [30]. 10 containers, each with a mass of $1.1\,\text{kg}$, were also selected to transport the samples [30].

2.2.5 Mars Descent Module

The MDM is in charge of landing payloads to the surface of Mars. This includes the ISRU plant, the SHAB and the MAV. The main components are summarised in Table 2.13, which was adapted from the DRA 5.0 Addendum II [31].

2.2.6 Mars Ascent Vehicle

The MAV ferries the crew from Mars surface back into the parking orbit, where it meets the THAB for the return trip. Choosing a more energetic orbit means that the THAB does not have to brake or accelerate as much when reaching or leaving Mars, respectively. However, it is also harder for the MAV to reach said orbit. The best compromise in order to alleviate the propellant needs of the THAB was a $250\,\text{km} \times 119\,450\,\text{km}$ orbit with a corresponding period of $5\,\text{sol}$ [30]. The resulting mass is summarised in Table 2.14.

Element	Mass, kg
Liquid oxygen	14 818
Liquid methane	4 939
Oxygen tanks	158
Fuel tanks	158
Main propulsion subsystem*	203.6
Six engines†	2 082.0
Structures	4 641.9
Thermal management*	636.7
Pressurant system*	289
RCS-Bipropellant*	249.1
Avionics*	544.7
EVA umbilical services*	8.3
Total (excluding payload)	28 728.3

* Extrapolated from Altair [31].
† Same engines as the MAV [31].

Table 2.13: MDM mass budget excluding the payload. Data adapted from [31]. Acronyms: Reaction Control System (RCS), Extravehicular Activity (EVA), Mars Ascent Vehicle (MAV) and Mars Descent Module (MDM).

2.2.7 In Situ Resource Utilisation

ISRU requirements are shown in Table 2.15. The driver for the ISRU system is dependent on its type. For atmospheric-based ISRU, only oxygen is produced. However, if regolith is mined as well, both oxygen and methane are produced at a mass ratio of 4:1 (assuming that a Sabatier reaction is employed) [11]. This is slightly higher than typical engine ratios, which vary between 3:1 and 3.5:1 [11]. Thus, excess oxygen is produced and the required methane drives the number of units needed.

Table 2.16 shows the characteristics of an ISRU unit for each type, and the corresponding mass and power requirements.

2.2.8 Surface Power System

Depending on the architecture chosen, there are two types of surface power system: solar or nuclear. For scenarios without ISRU (options A and B), the SHAB is the only power concern. Otherwise (options C and D), there are two phases: ascent propellant production, during which only the ISRU plant is being used, and crewed phase, where all propellant has already been produced and only the SHAB needs to be powered. ISRU power needs surpass by far the ones from the SHAB, thus being the driver.

Table 2.17 shows the mass budget for the surface power system. The values were obtained by extrapolating the data present in DRA 5.0 and include an extra $20\,\%$ contingency [5].

2.2.9 Re-Entry Capsule

Re-entry is typically limited by the amount of heat the spacecraft can dissipate, along with g-force limits for crewed missions. Since the interplanetary travel velocities are large for rapid missions, particular

Element	Mass, kg
Crew cabin	
Structures	1 303
Power	377
Avionics	241
Thermal	642
ECLSS	502
Cargo	808
Non-propellant fluids	295
Total	4 168
First stage	
Dry mass*	3 233
Liquid oxygen	19 352
Liquid methane	6 158
Total	28 742
Second stage	
Dry mass*	2 510
Liquid oxygen	8 616
Liquid methane	2 734
Total	13 859
MAV	
Total	46 769

* Includes engines and tanks [32].

Table 2.14: MAV liftoff mass for a 5 sol parking orbit. Data retrieved from [30], with cargo mass adapted for a crew of two. Acronyms: Mars Ascent Vehicle (MAV).

care needs to be taken when sizing the re-entry capsule.

In this analysis, the re-entry capsule was divided into non-TPS and TPS mass. The former is constant, while the latter varies with the re-entry velocity (dependent on the specific mission considered). The TPS mass fraction can then be defined as

$$\chi = \frac{m_{\text{TPS}}}{m_{\text{TPS}} + m_{\text{non-TPS}}}, \tag{2.3}$$

where χ is the TPS mass fraction, m_{TPS} is the mass of the TPS and $m_{\text{non-TPS}}$ is the mass of the non-TPS portion. The TPS mass fraction correlates well with the total heat load, and a fit based on historical data

ISRU type	Driver	Required mass, kg	Production rate, $\text{kg}\,\text{h}^{-1}\,\text{unit}^{-1}$	Required units*
Atmospheric-based	O_2	27 968	0.7	4
Atmospheric-based with regolith†	CH_4	8 892	0.2	4

* Assuming continuous production for 480 days [11].
† Assuming typical regolith, whose water content is 1.3 % [11] (worst-case scenario).

Table 2.15: ISRU units production rate. Data calculated from [11]. Acronyms: In Situ Resource Utilisation (ISRU).

ISRU type	Mass per unit, kg	Power per unit, kW	Total mass, kg	Total power, kW
Atmospheric-based	300.0	11.3	1 200.0	45.3
Atmospheric-based with regolith	566.7	17.3	2 266.7	69.3

Table 2.16: ISRU plant mass and power. The plant is composed by four units working in parallel. Unit data calculated from [11]. Acronyms: In Situ Resource Utilisation (ISRU).

Option	Mass, kg
A	5 838
B	5 423
C	10 450
D	13 450

Table 2.17: Surface power system mass budget.

for ablative shielding is given by [33]

$$\chi = 9.100 \times 10^{-4} \left(Q \times 10^{-4}\right)^{0.515\,75}, \tag{2.4}$$

where Q is the total heat load in $\mathrm{J/m^2}$.

Determining the exact heat load is not easy, and often requires a detailed simulation of the re-entry environment. For the scope of this work, a conservative estimate was done, which is meant to be refined by further work. The use of lift can open new re-entry trajectories [24], but is another convoluted topic. For the sake of simplicity, it was assumed that no lift was acting on the capsule and the ballistic re-entry equations of motion [29, 34] were numerically solved for the 1976 US Standard Atmosphere [29]. Then, both conductive [29] and radiative [35] heating rates were integrated to provide the total heat load. Apollo data [29, 33] was used as a benchmark since it is readily available and flight proven.

The afore analysis was repeated for several velocities at Earth infinity. For each, the arrival hyperbolic orbit impact parameter was varied as to provide the lowest TPS mass fraction possible. Overall, the re-entry heat load limit was given by Eq. (2.3) (since $\chi < 1$) while the g-force was set to a maximum of 8-g [20, 29]. The number of skips was left unconstrained as long as the spacecraft was captured in the end without crossing the afore mentioned thresholds. The resulting data can be seen in Table 2.18. For the remainder of the work, an interpolation of this data was used, which is shown graphically in Fig. 2.6. For a velocity of $11\,\mathrm{km/s}$, no solution was found. Therefore, for velocities larger than $10\,\mathrm{km/s}$, a propulsive braking was used to reduce it to this value.

2.2.10 Propellant

For propellant estimations, consider the rocket equation, given in non-dimensional form by [36]

$$\Delta v = -g I_{\mathrm{SP}} \log\left[\epsilon + (1-\epsilon)\varpi\right], \tag{2.5}$$

Velocity at Earth infinity, km/s	TPS mass fraction, %
7	31.2
8	37.7
9	46.5
10	58.5

Table 2.18: Velocity at Earth infinity and corresponding TPS mass fraction. Acronyms: Thermal Protection System (TPS).

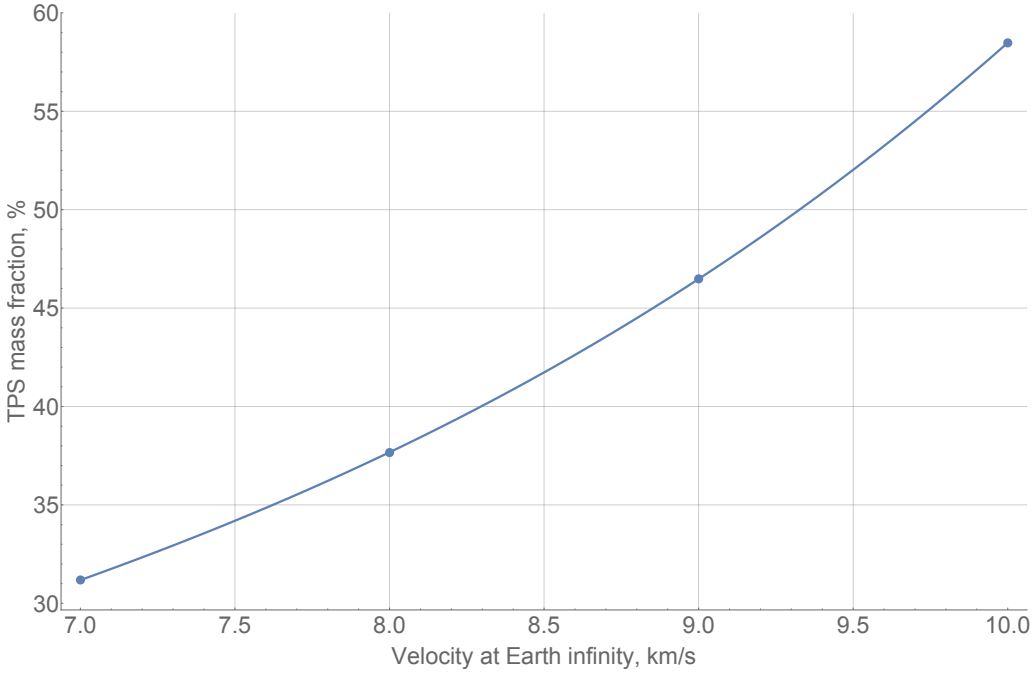

Figure 2.6: TPS mass fraction as a function of the velocity at Earth infinity. Acronyms: Thermal Protection System (TPS).

where Δv is the total change in velocity, g is the gravitational acceleration at Earth's surface ($9.806\,7\ \mathrm{m/s^2}$ [29]), I_{SP} is the specific impulse of the engine, $\epsilon = m_s/(m_s+m_p)$ is the structural ratio, m_s is the structural mass, m_p is the propellant mass, $\varpi = m_*/m_0$ is the payload ratio, m_* is the payload mass and m_0 is the mass at the start of the manoeuvre.

Finite burn losses can be incorporated as

$$\Delta v = \Delta v_{\mathrm{ideal}} + \Delta v_{\mathrm{losses}}, \tag{2.6}$$

where $\Delta v_{\mathrm{ideal}}$ is the ideal change in velocity (from an impulsive manoeuvre) and $\Delta v_{\mathrm{losses}}$ is the extra amount needed to compensate the losses. An estimate of the latter is given by [37, 38]

$$\Delta v_{\mathrm{losses}} = \frac{1}{24}\frac{\mu}{r^3}{t_{\mathrm{burn}}}^2 \Delta v_{\mathrm{ideal}}, \tag{2.7}$$

where μ is the gravitational parameter of the primary, r is the distance to the primary when executing the impulsive manoeuvre and t_{burn} is the time for the propellant to be burnt. This is a conservative estimate,

since actual burn losses can be smaller by up to a factor of two [38]. The burn time is a function of the propellant mass through [38]

$$t_{\text{burn}} = \frac{gI_{\text{SP}}}{T} m_p, \tag{2.8}$$

where T is the thrust. Using Eqs. (2.5) to (2.8), the modified rocket equation can be written as

$$\Delta v_{\text{ideal}} \left[1 + \frac{1}{24} \frac{\mu}{r^3} \left(\frac{gI_{\text{SP}}}{T} \right)^2 {m_p}^2 \right] = -gI_{\text{SP}} \log \left[\epsilon + (1-\epsilon)\varpi \right]. \tag{2.9}$$

In order to include the gains from the disposal of empty propellant tanks, an analogy was made with a rocket with N stages [36]. For that end, the structural ratio and payload ratio of the k-th stage is defined as

$$\epsilon_k = \frac{m_{sk}}{m_{sk} + m_{pk}} \tag{2.10}$$

and

$$\varpi_k = \frac{m_{0k+1}}{m_{0k}}, \tag{2.11}$$

where m_{sk} is the structural mass of the k-th stage, m_{pk} is the propellant mass of the k-th stage, m_{0k+1} is the initial mass of the stage $k+1$ and m_{0k} is the initial mass of the stage k. Assuming that the same tank technology is used for every stage, the structural ratio is also the same [36]. This result is independent of the relation between tank mass and propellant mass. But in order to calculate the structural factor, it was also assumed that the tank mass was proportional to the propellant mass. In principle, it should be proportional to the two-thirds power of the latter, since it scales with the tank surface area instead of the tank volume. However, the deposits arrangement and connections should also be more complex as the number of tanks increases, leading to higher masses. In order to take a conservative approach, the linear relation[5] was kept. In this case, the structural ratio is given by

$$\epsilon_k = \frac{K m_{pk}}{K m_{pk} + m_{pk}} = \frac{K}{K+1}, \tag{2.12}$$

where K is the constant of proportionality. Data retrieved for common chemical propellants[6] and propellant tanks [7] resulted in $K \approx 0.040$. Assuming that the propellant tanks all have the same size,

$$m_{pk} = \frac{m_p}{N}, \tag{2.13}$$

where m_{pk} is the propellant mass of the k-th stage. Since the payload of the k-th stage is the initial mass of stage $k+1$, it is possible to find recurrence relations by accounting the initial mass, propellant mass, structural mass and payload mass of the k-th stage. Using Eqs. (2.10) and (2.11), they can be re-written in terms of the stage structural and payload ratios. It can then be shown that the closed-form

[5] This type of linear relation has also been used in other works [39].

[6] Braeunig, R. A., "Rocket Propellants," `http://www.braeunig.us/space/propel.htm`, 2008. Retrieved 17 December 2020.

[7] Astrium, "Propellant Tanks for Spacecraft," `https://www.yumpu.com/en/document/view/17516891/propellant-tanks-for-spacecraft-astrium-st-service-portal-eads`, 2013. Retrieved 15 December 2020.

solution for the k-th stage payload ratio is given by

$$\varpi_k = \frac{m_*(1-\epsilon) + (N-k)m_p/N}{m_*(1-\epsilon) + (N-k+1)m_p/N}, \tag{2.14}$$

when the tanks are equal, i.e. same technology and size. Since Eq. (2.9) is applicable to each stage, the overall change in velocity can be written as

$$\begin{aligned}\Delta v_{\text{ideal}} \left[1 + \frac{1}{24}\frac{\mu}{r^3}\left(\frac{gI_{\text{SP}}}{T}\right)^2 {m_p}^2\right] = -gI_{\text{SP}}\left(1 + \frac{1}{24}\frac{\mu}{r^3}\frac{g^2{I_{\text{SP}}}^2}{T^2}\frac{{m_p}^2}{N^2}\right)^{-1} \times \\ \times \sum_{k=1}^{N} \log\left(\epsilon + (1-\epsilon)\frac{Nm_*(1-\epsilon) + (N-k)m_p}{Nm_*(1-\epsilon) + (N-k+1)m_p}\right).\end{aligned} \tag{2.15}$$

In the context of rapid missions, propellant mass is expected to be considerable. Thus, a high number of propellant tanks of regular size can be used. Equation (2.15), can be re-written in terms of the Gamma function [40] and the limit when N tends to infinity taken, leading to

$$m_p = m_*(1-\epsilon)\left(\exp\left[\frac{1}{1-\epsilon}\frac{\Delta v_{\text{ideal}}}{gI_{\text{SP}}}\left(1 + \frac{1}{24}\frac{\mu}{r^3}\frac{g^2{I_{\text{SP}}}^2}{T^2}{m_p}^2\right)\right] - 1\right). \tag{2.16}$$

This is similar to the traditional rocket equation expressing the propellant mass,

$$m_p = m_f\left[\exp\left(\frac{\Delta v}{gI_{\text{SP}}}\right) - 1\right], \tag{2.17}$$

where m_f is the mass at the end of the manoeuvre, but accounts for both the tank mass (assuming each tank is disposed when empty and small enough for the continuous approximation to be valid) and finite burn losses. Thus, Eq. (2.16) was used throughout the work for the propellant estimations.

2.3 Manoeuvres

The THAB is mainly subject to four manoeuvres: at Earth departure, Mars arrival, Mars departure and Earth arrival. The required changes in velocity for the interplanetary trajectory (for the considered high-thrust scenario) are the solution to a Lambert's problem with co-planar circular orbits.

The mission starts from a circular Low Earth Orbit (LEO) with an altitude of $500\,\text{km}$, considered to be a good starting point and comparable with the literature [16]. In order to reduce departure gravity losses, two apogee raising manoeuvres are performed before placing the THAB in the escape trajectory. This assures that the burn loss estimation is valid but likely overestimated.

When reaching Mars, the THAB is placed into a parking orbit via a propulsive braking at the periapsis of the arrival orbit. Mars departure is achieved in an analogous way. In this case, no apogee raising manoeuvres are needed since the parking orbit is already quite energetic.

For the return trip, a maximum allowed velocity at Earth infinity of $10\,\text{km/s}$ (corresponding to a re-entry velocity of about $14.927\,\text{km/s}$) was defined following the analysis of Section 2.2.9. For higher incoming velocities, additional propulsive braking is required. In this case, the perigee is inside Earth's

atmosphere. A propulsive braking at such location may be difficult or even infeasible. On the other hand, braking at Earth infinity is inefficient but allows for plenty of time to execute the manoeuvre and perform security checks. A compromise between the two extremes is likely the optimum solution, but an in-depth analysis is required (which may, eventually, be dependent on the detailed design). Thus, it was opted to brake at Earth infinity for both simplicity and to be conservative.

Chapter 3

Propulsion

3.1 Overview

In this work only impulsive manoeuvres were considered, which corresponds to a high-thrust scenario. The case of continuous thrust manoeuvres will be analysed in a future work.

Propulsion systems are characterised by two parameters: specific impulse and thrust-to-weight ratio. The first is a measure of its efficiency, while the latter expresses its acceleration in multiples of Earth's gravitational acceleration. Thrust itself is not characteristic of the system since engines can be, to a certain degree, added in parallel. Figure 3.1 shows these two parameters for several modern and proposed propulsion systems [41]. Chemical systems are characterised by a high thrust-to-weight ratio

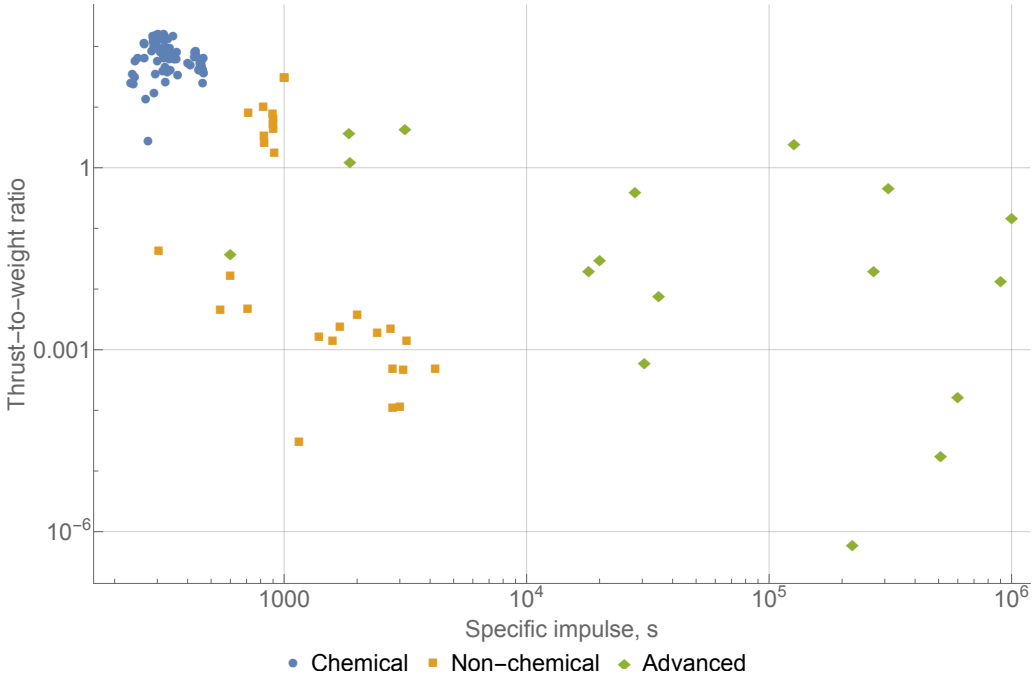

Figure 3.1: Specific impulse and thrust-to-weight ratio for several modern and proposed propulsion systems. Blue dots, orange squares and green diamonds represent chemical, non-chemical and advanced systems, respectively. Data retrieved from [41].

but relatively low specific impulse. These are at least at a TRL of six. Non-chemical systems (for instance electrical), are more efficient but tend to produce smaller accelerations. Although some are at a TRL of nine, others can be as low as three. Lastly, advanced systems values do not follow a specific trend. Available information is estimated since the TRL is, at most, three.

3.2 Representative Values for High-Thrust Propulsion Systems

In order to select representative values for the propulsion system parameters, points with highest thrust-to-weight ratios for a given specific impulse (corresponding to the high-thrust scenario) were identified in Fig. 3.1. A linear regression (in logarithmic scale) was then made, and optimistic and pessimistic curves were drawn. These were shifted vertically by a symmetric amount regarding the regression. Finally, points were chosen at regular[1] specific impulse intervals, with the corresponding thrust-to-weight ratios being rounded for ease in display. The results are shown in Fig. 3.2, with expressions given by

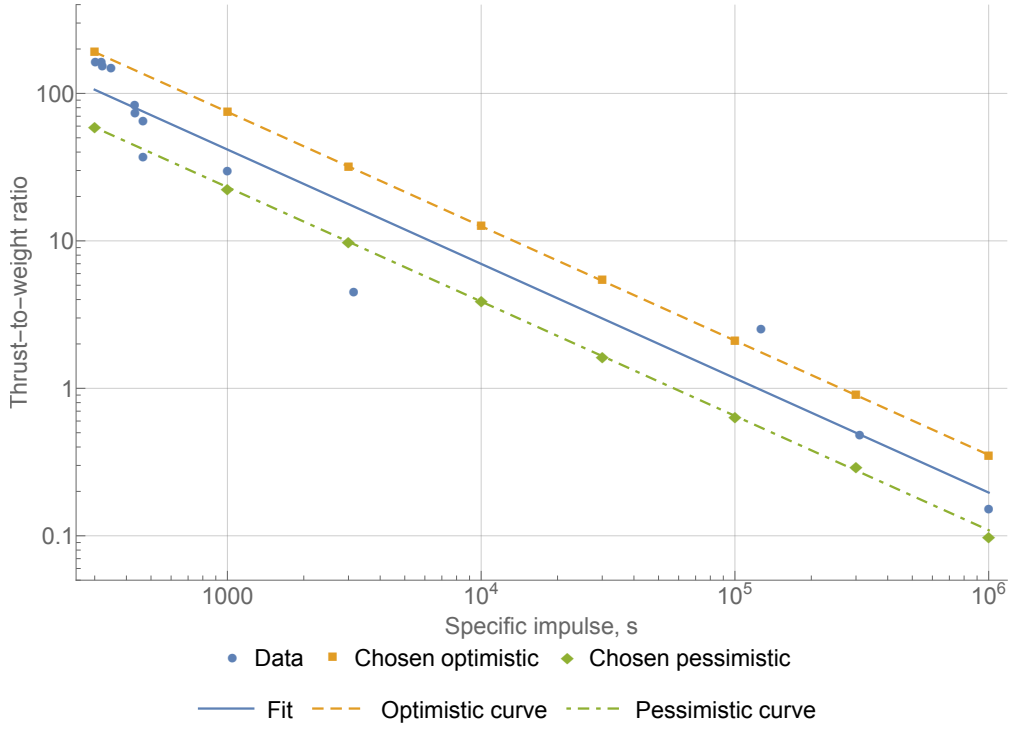

Figure 3.2: Most promising propulsion systems (blue dots) and corresponding regression (blue full line). Optimistic and pessimistic curves (orange dashed and green dash-dotted lines, respectively) obtained by a symmetric amount of vertical shifting regarding the regression. Orange squares and green diamonds are the chosen optimistic and pessimistic representative values, respectively.

$$T/W = c{I_{\text{SP}}}^{-0.775}, \tag{3.1}$$

where T/W is the thrust-to-weight ratio, I_{SP} is the specific impulse in s and c is 8 826.177, 15 887.118 and 4 903.431 for the regression, optimistic curve and pessimistic curve, respectively.

[1] Specific impulse values were chosen in the format $a \times 10^b$, with $a \in \{1, 3\}$ and $b \in [2, 6]$. Since a logarithmic scale was used, values in the form 3×10^b sit approximately in the middle of 10^b and 10^{b+1}.

3.3 Cases Studied and Assumptions

Originally, this work intended to analyse all of the 16 cases chosen as representative values for the parameters of high-thrust propulsion systems. However, the number had to be limited to five due to time constraints. In these circumstances, the left-most (in Fig. 3.2) optimistic points were kept. For ease of reference, these were summarised in Table 3.1. It makes sense to start with the left-most points since

Case	Specific impulse, s	Thrust-to-weight ratio
I	3×10^2	190.0
II	1×10^3	75.0
III	3×10^3	32.0
IV	1×10^4	12.6
V	3×10^4	5.4

Table 3.1: Studied values for the propulsion system parameters.

these correspond to a higher TRL. At the same time, this work took a conservative approach on most topics that required further study. If values from the pessimistic curve were taken instead, the results could have been too overestimated. Nonetheless, all the cases will be investigated in a future work. But for a first impression, the optimistic ones were deemed more useful.

Besides the unstudied cases from Section 3.2, propulsion systems with lower thrust-to-weight ratios will also be studied in future works. These are not adequate for an impulsive approach, but may be useful in a continuous thrust scenario. This requires a different approach than the Lambert's solver employed in this work, and should be studied separately.

The systems shown in Fig. 3.1 cover the whole TRL range, from one to nine. In particular, systems categorised as advanced have notoriously low TRL values, implying that the values are speculative and uncertain. It may seem unrealistic to include them in such analysis, but there is merit in doing so. With the propulsion of today, rapid trips to Mars require large amounts of propellants that lead to exceedingly high values for IMLEO. Will this paradigm change? Does any of the currently proposed systems, even if somewhat far-fetched, enable rapid travels with reasonable mass? These are the type of questions that can be answered by encompassing these systems.

Lastly, two important assumptions were made. First, it was considered that engines could be added in parallel in order to ensure the high-thrust required for the impulsive scenario. This essentially turns the thrust (or equivalently the number of engines) into a design parameter, which can be varied to yield the best result. Second, some propulsion systems also require a separate power source. When applicable, and unless otherwise stated by the source, it was considered that this was included in the thrust-to-weight ratio of the system.

Chapter 4

Results

The trade-off between IMLEO and total trip time (proxies for cost and risk, respectively) is considered for several architectures. Each includes a distinct combination of the options referred in Table 2.4 with the propulsive systems selected in Table 3.1, for a total of 20. Only rapid trips with short stays were studied, in order to avoid the long waiting times associated with longer, more economic missions. This way, the exposure to radiation and reduced-gravity environments is minimised.

Code-wise, the algorithm has four inputs, namely an option from Table 2.4, specific impulse, thrust-to-weight ratio and duration of the stay. These correspond to selecting one of the afore mentioned architectures. Due to time constraints, only a stay of $30\,\mathrm{d}$ was considered (consistent with the duration mentioned in the DRA 5.0 for short-stay missions [5]) but more will be analysed in a future work. For each input combination, there are four free parameters which can varied to yield the lowest output (i.e. IMLEO) for a certain total trip time: thrust, time of departure, duration of the outbound travel, and duration of the return travel. All times were counted from an opposition[1] configuration. Time resolution was variable, depending on the needs, but was no higher than $1\,\mathrm{d}$.

In the following results, the total trip time includes the stay time. Although the adverse effects, from radiation [42] and reduced gravity [43], are slightly reduced in Mars, they still pose a considerable risk. Since the results are meant to be a proxy of the trade-off between cost and risk, all the exposure time must be accounted for, and not just the time spent travelling between the planets. IMLEO was also capped at $10^5\,\mathrm{t}$. Although this might seem excessive for today's standards, it is meant to give a perspective of what might be achievable in the future. Typically, IMLEO can go up to around $1\,000\,\mathrm{t}$ [4, 5] but there is an effort to reduce launch costs by a factor of 100[2]. Thus, an IMLEO of $100 \times 10^3\,\mathrm{t} = 10^5\,\mathrm{t}$ might become reasonable.

[1] This is the time in which the Sun, Earth and Mars are in a straight line, with Mars and the Sun in opposite positions when seen from Earth [1].

[2] Galeon, D., "Elon Musk: With New SpaceX Tech, Rocket Costs Will Drop by a Factor of 100," `https://futurism.com/elon-musk-with-new-spacex-tech-rocket-costs-will-drop-by-a-factor-of-100`, September 2017. Retrieved 30 December 2020.

4.1 General Shape of the Pareto Front

In order to understand the relation between the best IMLEO (for each total trip time) and the total trip time, under the assumptions of this work, an example of the corresponding Pareto front is shown in Fig. 4.1. For longer missions, IMLEO variations are small. But as the round trip time starts decreasing,

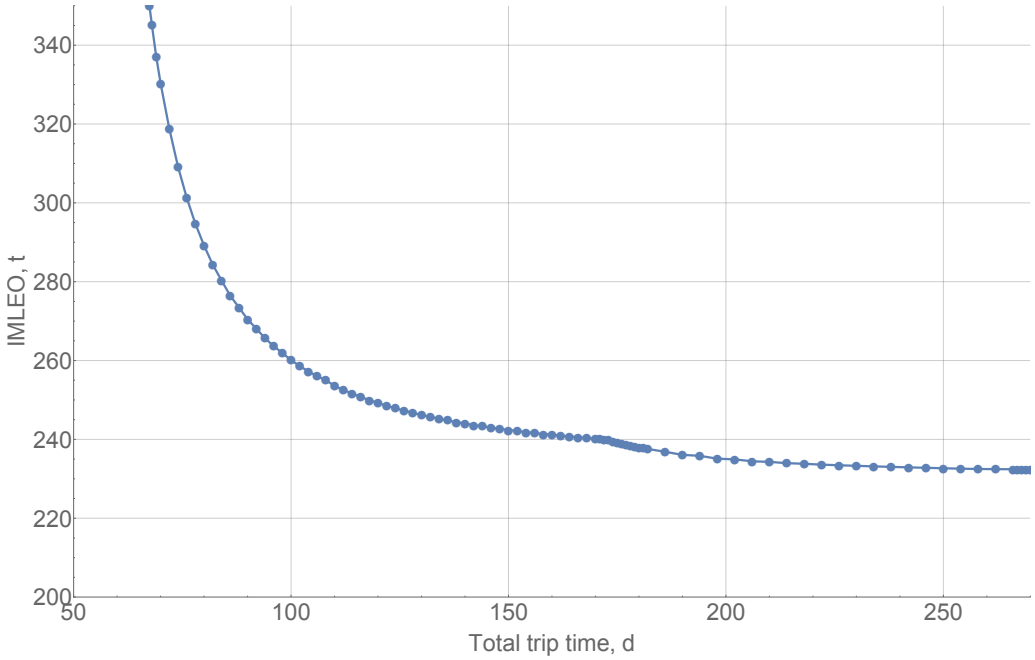

Figure 4.1: Pareto front for option C and propulsion case IV, with a stay time of 30 d. IMLEO range was cropped to show the derivative discontinuity. Acronyms: Initial Mass in Low Earth Orbit (IMLEO).

the curve gets steeper and steeper. This behaviour implies there is a mathematical limit to the minimum travel time, which is due to the burn losses term in Eq. (2.16). Unlike the traditional rocket equation, there is no guarantee that a solution, for the propellant mass, exists for every combination of values. Furthermore, each scenario also has a practical limit, for which it is not worthwhile to try do decrease the total trip time further due to the high steepness of the curve.

The other interesting feature is the discontinuity in the derivative, which occurs around the 170 d mark for the given example. This signals the need of a propulsive braking manoeuvre when approaching Earth, as mentioned in Section 2.3. Although this is present in every case, the variation is small and can be easily masked when showing a larger IMLEO range.

4.2 Influence of the Specific Impulse and Thrust-to-Weight Ratio

Although all of the studied cases display the same behaviour mentioned in Section 4.1, there are, naturally, significant changes to minimum travel time, IMLEO range and IMLEO for longer missions, depending on the selected propulsion system. The Pareto fronts for each case (recall Table 3.1) are shown in Figs. 4.2 to 4.5, for options A, B, C and D (recall Table 2.4), respectively.

For propulsion case I, only a section of the curve appears since even for the largest times considered,

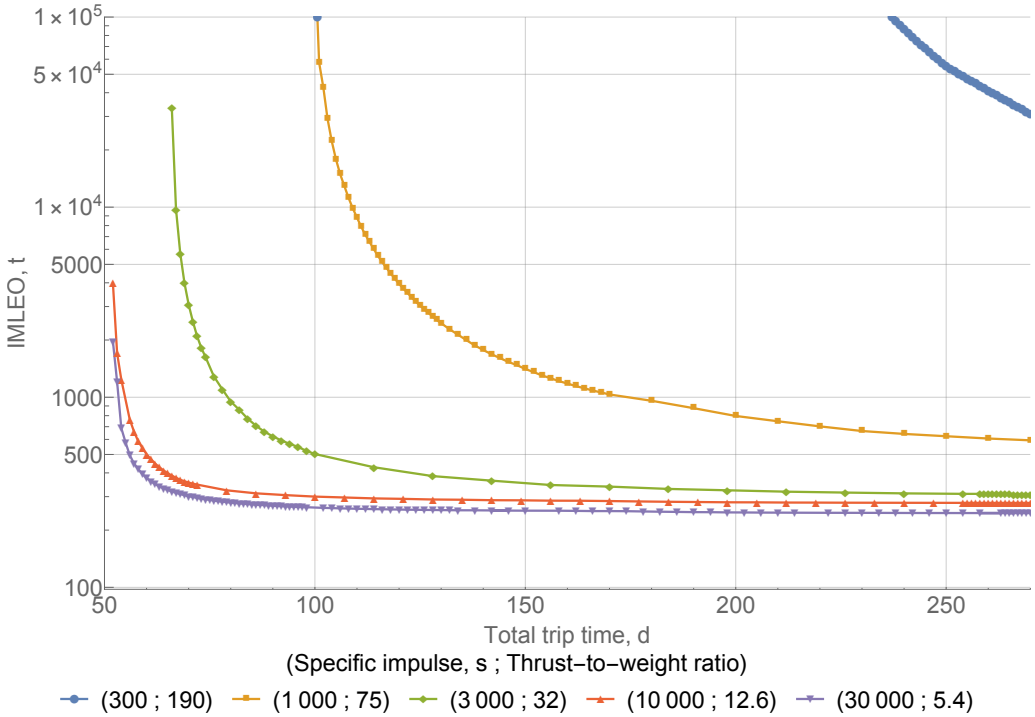

Figure 4.2: Pareto fronts for option A and propulsion cases I through V, with a stay time of 30 d. Blue dots, orange squares, green diamonds, red upright triangles and purple inverted triangles correspond to propulsion cases I, II, III, IV and V, respectively. Acronyms: Initial Mass in Low Earth Orbit (IMLEO).

the IMLEO ranges from about 3×10^4 t to 10^5 t. The remaining cases feature the vast majority of the curve despite cases III through V not reaching the cap of 10^5 t (a resolution higher than 1 d was needed).

When progressing from propulsion cases I through V, the best IMLEO for a certain time starts decreasing. This variation is large at first, but it gets progressively smaller. For 250 d, for instance, compare the massive reduction from about 6×10^4 t to about 700 t (from case I to case II) with the less significant reduction from the latter to about 300 t (from case II to case III). From case III onwards, the gains in IMLEO are even smaller. Furthermore, the gains are larger for faster trips.

The gains in minimum total trip time exhibit a similar behaviour to those in the IMLEO. For propulsion case I, the minimum total trip time is not present in the plots since it leads to masses higher than 10^5 t. From cases II to IV, it is about 100 d, 65 d and 50 d, respectively. Case V shares the same minimum total trip time of case IV.

From the above results, it can be concluded that propulsion case I does not fit the rapid mission archetype. Since this case is mostly representative of today's propulsion technology limits, rapid missions are likely not yet achievable with a reasonable IMLEO.

In order to explain the lower gains when progressing from propulsion cases I through V, first it is useful to closely inspect Eq. (2.16), re-written here for convenience

$$m_p = m_*(1-\epsilon)\left(\exp\left[\frac{1}{1-\epsilon}\frac{\Delta v_{\text{ideal}}}{gI_{\text{SP}}}\left(1+\frac{1}{24}\frac{\mu}{r^3}\frac{g^2{I_{\text{SP}}}^2}{T^2}{m_p}^2\right)\right]-1\right).$$

Specifically, the effects of thrust, specific impulse and thrust-to-weight ratio. These are enclosed in Eq. (2.16), despite other elements contribution to the IMLEO.

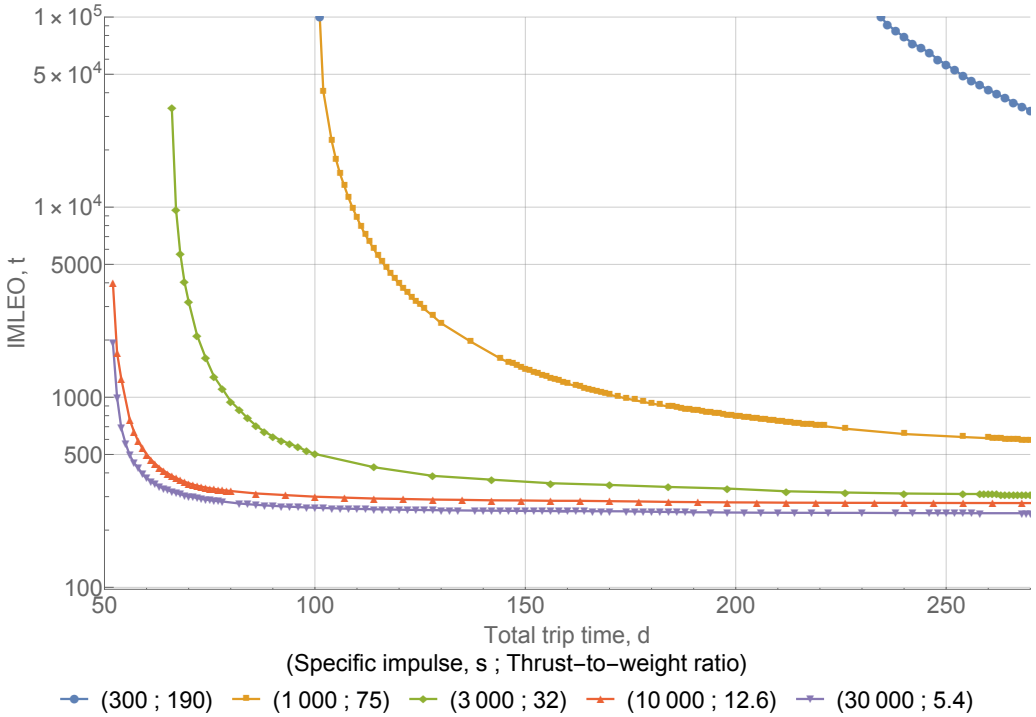

Figure 4.3: Pareto fronts for option B and propulsion cases I through V, with a stay time of 30 d. Blue dots, orange squares, green diamonds, red upright triangles and purple inverted triangles correspond to propulsion cases I, II, III, IV and V, respectively. Acronyms: Initial Mass in Low Earth Orbit (IMLEO).

Thrust impacts the equation in two ways: a direct decrease in the argument of the exponential and an indirect increase in the payload mass of the manoeuvre through the propulsion system mass. The latter is adverse, and the effect is more severe the lower the thrust-to-weight ratio. The former is trickier to analyse, since this is an implicit equation for the propellant mass, without a closed form solution. For reasonable values, the burn losses can be made small by increasing the thrust, which means that

$$\frac{1}{24}\frac{\mu}{r^3}\frac{g^2 {I_{\text{SP}}}^2}{T^2}{m_p}^2 \ll 1, \tag{4.1}$$

and a closed form approximation is obtained,

$$m_p \approx m_*(1-\epsilon)\left[\exp\left(\frac{1}{1-\epsilon}\frac{\Delta v_{\text{ideal}}}{g I_{\text{SP}}}\right) - 1\right]. \tag{4.2}$$

The reduction of burn losses is beneficial albeit limited, since they can only be null, at best. However, as the thrust increases, so does the propellant mass. After a certain point, the latter is comparable to the former, and Eq. (4.1) no longer holds (notice that the burn losses term is also proportional to the square of propellant mass). Thus, there must be an optimal value for thrust. Indeed, this was experienced when obtaining the Pareto fronts, and a graphical example is shown in Fig. 4.6.

Specific impulse has two contrary effects on the argument of the exponential term in Eq. (2.16), since a part of it is proportional to the specific impulse while the other is proportional to the inverse. Equation (4.2) holds for low values of specific impulse, where it is beneficial to increase it (much like the

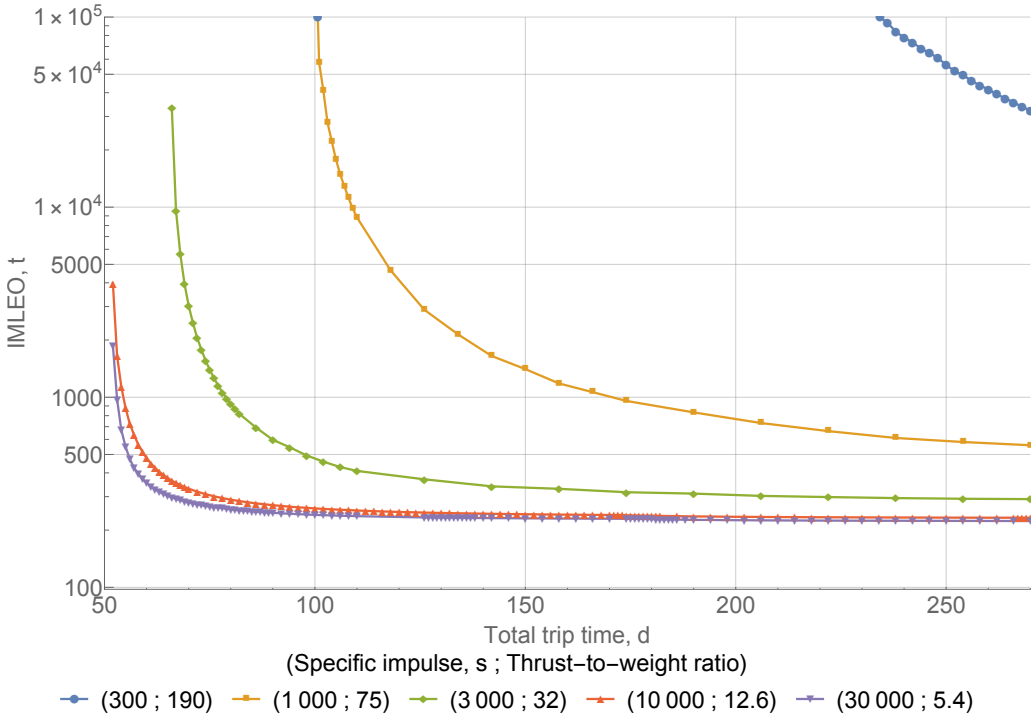

Figure 4.4: Pareto fronts for option C and propulsion cases I through V, with a stay time of 30 d. Blue dots, orange squares, green diamonds, red upright triangles and purple inverted triangles correspond to propulsion cases I, II, III, IV and V, respectively. Acronyms: Initial Mass in Low Earth Orbit (IMLEO).

traditional rocket equation). However, the burn loss term should dominate for higher values, resulting in

$$m_p \approx m_*(1-\epsilon)\left[\exp\left(\frac{1}{24}\frac{\Delta v_{\text{ideal}}}{1-\epsilon}\frac{\mu}{r^3}\frac{gI_{\text{SP}}}{T^2}{m_p}^2\right)-1\right], \tag{4.3}$$

for which increases in specific impulse clearly have a negative impact in the propellant mass. Nonetheless, the example of Fig. 4.7 (the same as the one featured in Fig. 4.6, but with constant thrust and variable specific impulse instead) only shows the propellant mass decrease with the inverse of the specific impulse. Thus, increasing the specific impulse seems to be, overall, beneficial.

Thrust-to-weight ratio has the simplest influence. Essentially, the higher the ratio the lower the payload mass of the manoeuvre, which contributes to a lower propellant mass, if a solution exists, or to the existence of the solution, otherwise.

When combining these effects with the results described, it can be inferred that when progressing from propulsion cases I through V, the beneficial effects (i.e. increasing the specific impulse) dominate at first. However, these eventually become comparable with the adverse effects. The latter seem to be due to the decrease in the thrust-to-weight ratio, since Fig. 4.7 seems to indicate that the specific impulse is never high enough to have a negative impact. This has been verified for this example (with fixed thrust and departure, outbound, stay and return times), but a larger simulation with the specific impulse freed as a parameter should be carried, in a future work, to grasp the full effect on IMLEO.

For the unstudied propulsion systems with specific impulses higher than 3×10^4 s (displayed in Fig. 3.2), it is expected that the curves will either converge (if positive effects stay superior to the negative ones), or invert the tendency and start yielding worse results (if the negative effects of decreasing

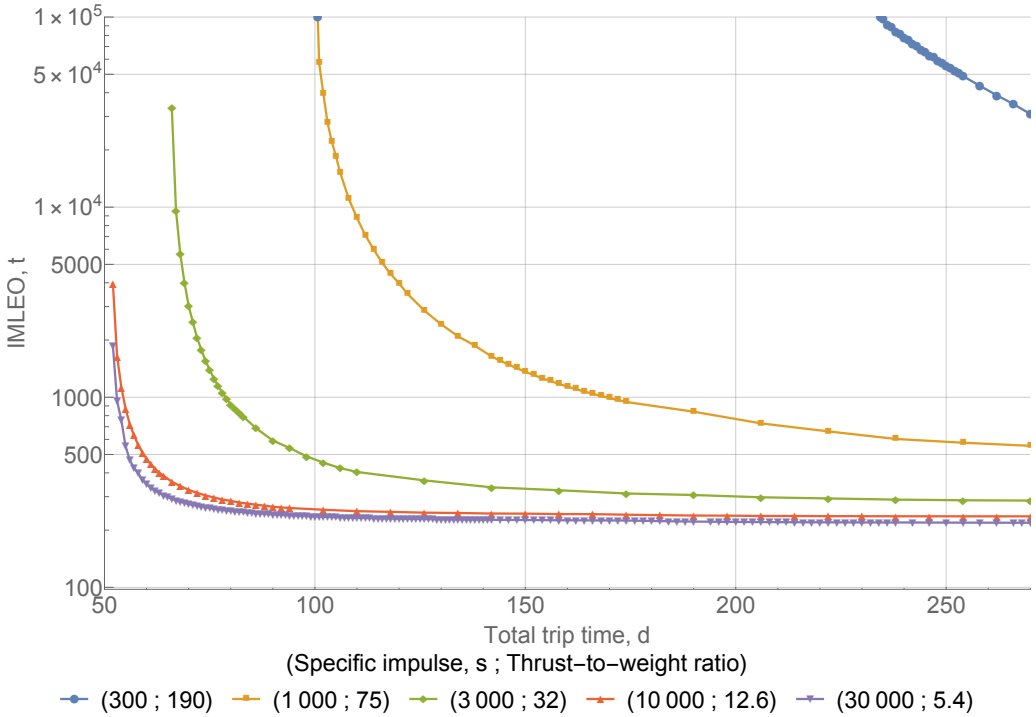

Figure 4.5: Pareto fronts for option D and propulsion cases I through V, with a stay time of 30 d. Blue dots, orange squares, green diamonds, red upright triangles and purple inverted triangles correspond to propulsion cases I, II, III, IV and V, respectively. Acronyms: Initial Mass in Low Earth Orbit (IMLEO).

the thrust-to-weight ratio eventually dominate).

4.3 Comparison Between Architectures

In order to compare the studied architectures, Figs. 4.2 to 4.5, were plotted together in Fig. 4.8. The figure is a little confusing, but that itself is the key point to be taken. Differences in the studied options (Table 2.4) have minor influences, which only become noticeable when the curves start to flatten. This happens because, for faster missions, a higher portion of the IMLEO is constituted by propellant mass. Thus, the analysed options are more relevant for minimum-energy transfers, where the mass is more evenly distributed between elements, than for rapid round trips, where most of the mass stems from the propellant. The effect may appear more prominent for higher specific impulses, but that stems from the logarithmic scale used in the plots. Overall, architectures are mostly dependent on the characteristics of the propulsion system.

It is important to recall that ISRU is only being considered for the production of ascent propellant. In fact, were it possible to produce the return fuel on Mars, IMLEO could be significantly lower. This should be addressed in a future work as it requires major changes in the architecture.

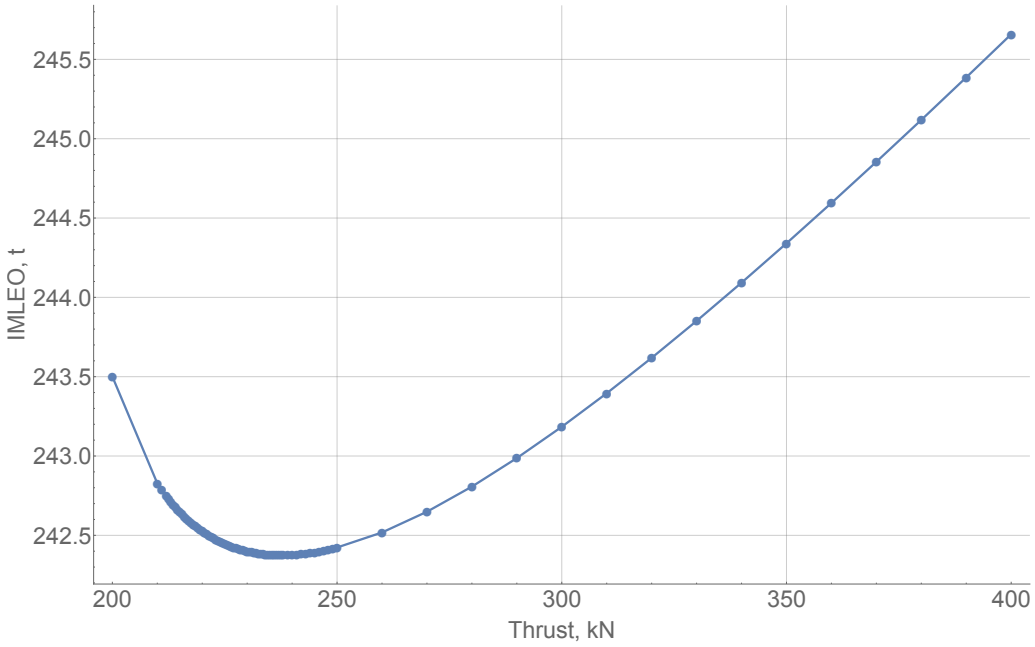

Figure 4.6: Effect of thrust on IMLEO. Example for option C and propulsion case IV, for an outbound travel time, stay time, return travel time and departure time of 60 d, 30 d, 60 d and 680 d, respectively. Acronyms: Initial Mass in Low Earth Orbit (IMLEO).

4.4 Relation Between Outbound and Return Travel Times

Besides the IMLEO, it is also interesting to analyse the relation between outbound and return travel times. This is shown in Figs. 4.9 to 4.12 for options A, B, C and D, respectively.

It can be seen that the relation is approximately linear, with slightly faster outbound travels. Since all the propellant for the return trip must first be carried to Mars, it is less expensive to accelerate the outbound trip rather than the return one. Unsurprisingly, this holds for every propulsion case and every option since it is only related to the geometry of the interplanetary trajectories.

As a side note, the points start to disperse for larger times. This is likely due to the lower parameter resolution that was used for calculations in that area. Although it was enough to obtain satisfying results for the IMLEO, it might not have been enough to establish this relation in those cases.

4.5 Implications for Rapid Missions to Mars

The unfavourable results for the propulsion case I, representative of today, indicate that rapid missions may not yet be achievable with a reasonable mass. However, the results are encouraging for the near future. In particular, the DRA 5.0 states an IMLEO of 849 t for a total trip time of 916 d. Even if one does not account for the large stay of 496 d [5], it still features a trip of 420 d. For the propulsion case II, the one most likely to be available in the near future, a mission with similar mass can be undertaken in about 200 d, corresponding to a trip of about 170 d. This corresponds approximately to a 59.5 % decrease in travel time (excluding stay), or a 78.2 % decrease in total trip time. The time can be decreased further, for propulsion cases III through V, but each case is farther away in the future.

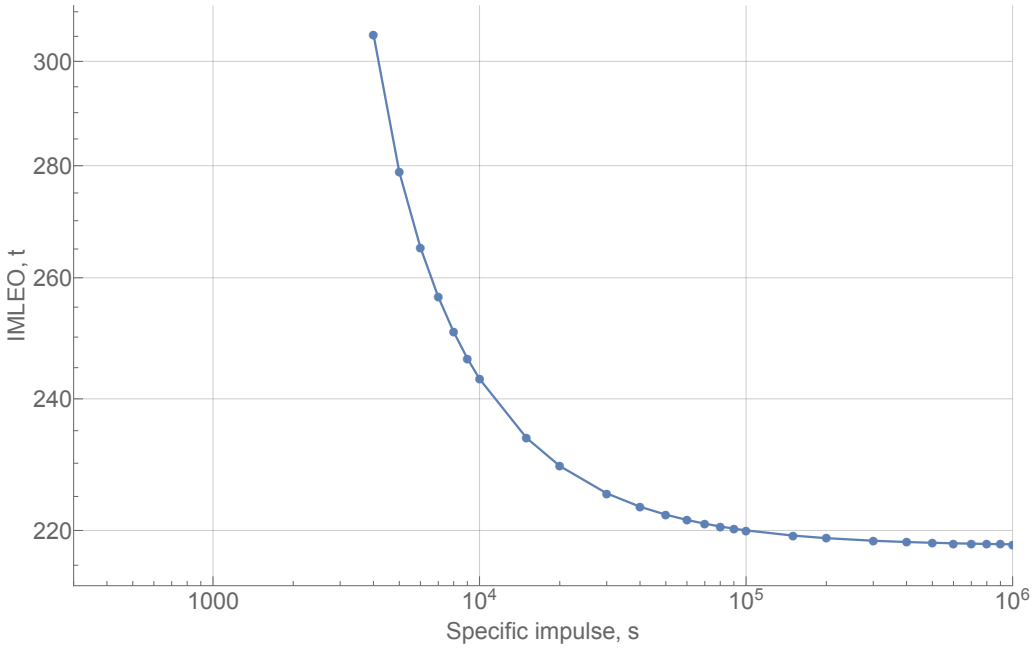

Figure 4.7: Effect of specific impulse on IMLEO. Example for option C, for a thrust-to-weight ratio, thrust, outbound travel time, stay time, return travel time and departure time of 12.6, 300 kN, 60 d, 30 d, 60 d and 680 d, respectively. Acronyms: Initial Mass in Low Earth Orbit (IMLEO).

Overall, rapid crewed missions to Mars are likely to become competitive with the traditional minimal-energy approach. Nonetheless, there are aspects that would benefit from better estimations while others were not pursued in this work. The former encompasses the re-entry portion of the mission (in need of a detailed simulation in the range applicable to rapid missions), the burn losses (in need of a more accurate analytical expression, or simulations in the desired range) and the propulsion system mass (including better estimations for the tank mass and number, as well the required elements for advanced systems). The latter encompasses the use of aerocapture at Mars, the location of the propulsive braking when approaching Earth, and the use of ISRU for the production of return propellant. The last, in particular, is expected to require large changes to the architecture, as well as a way to store the propellant for a large amount of time.

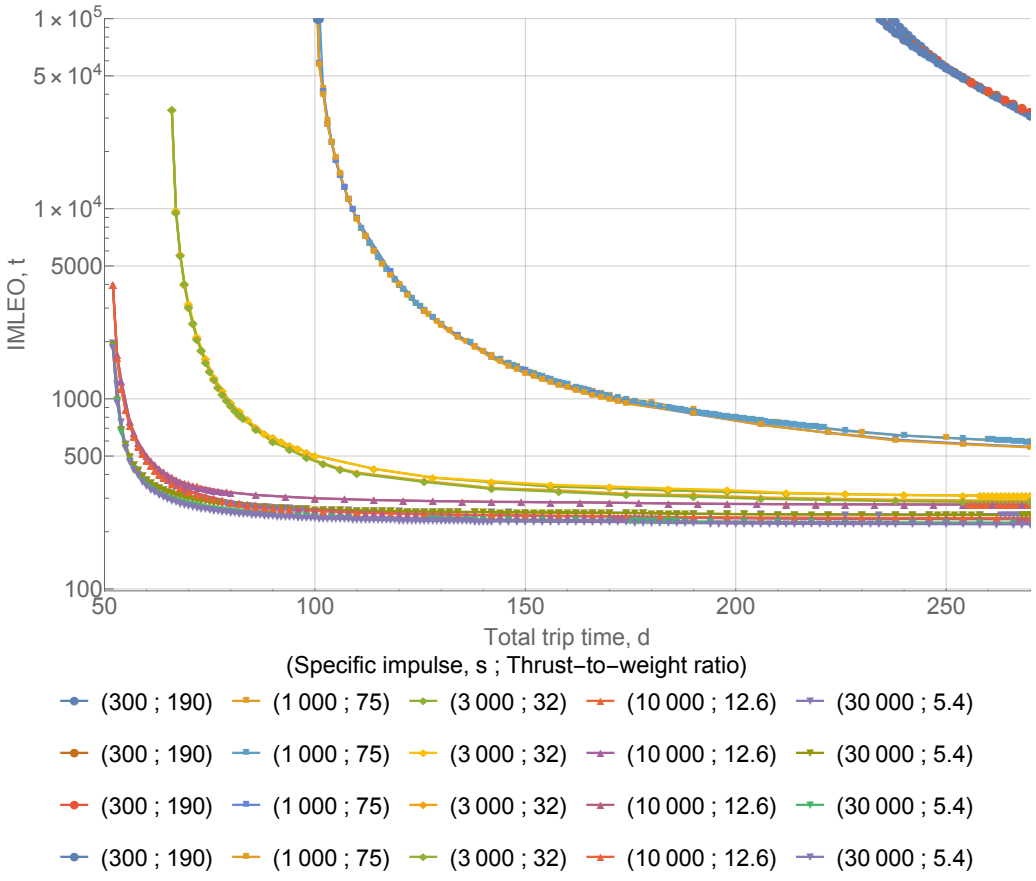

Figure 4.8: Pareto fronts for options A through D and propulsion cases I through V, with a stay time of 30 d. The first, second, third and fourth row in the legend correspond to options A, B, C and D, respectively. Acronyms: Initial Mass in Low Earth Orbit (IMLEO).

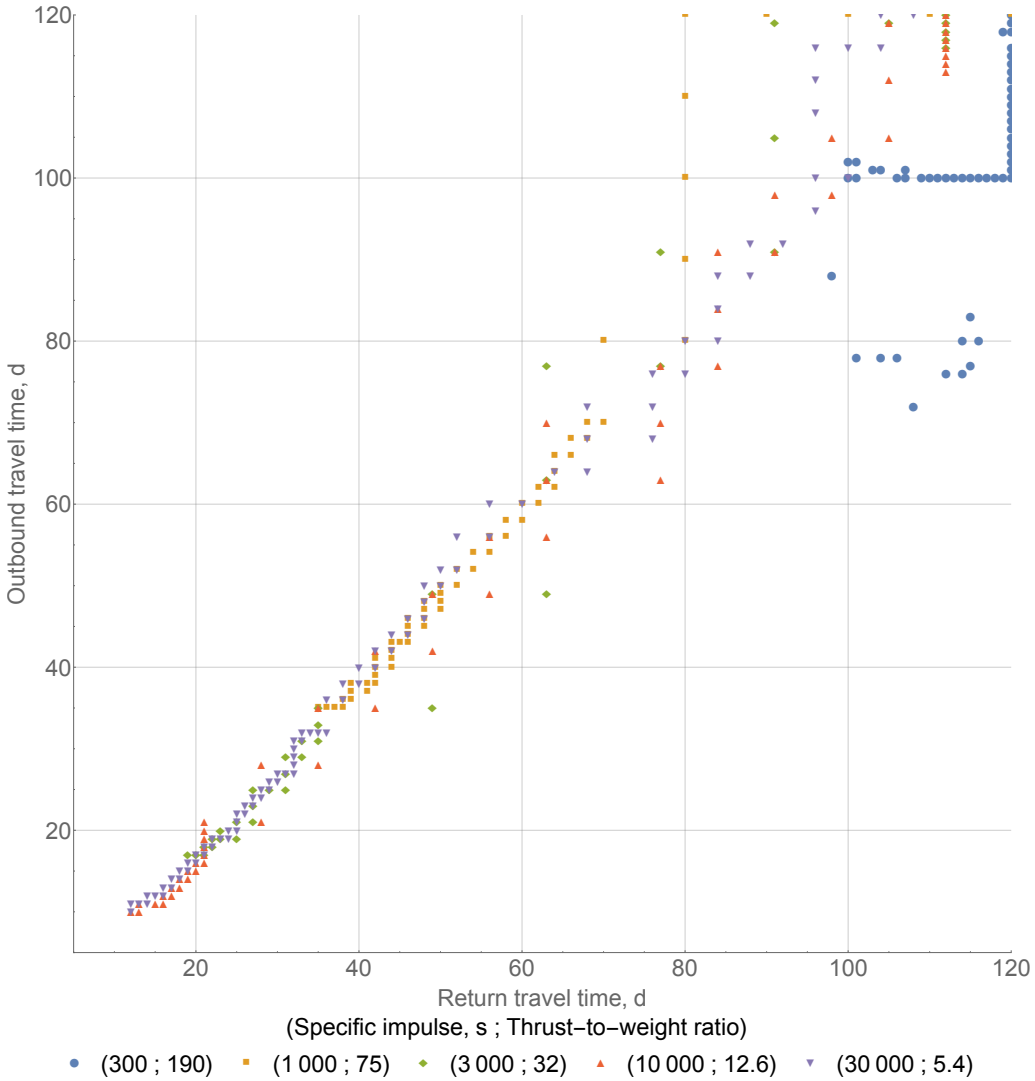

Figure 4.9: Relation between outbound and return travel times for option A and propulsion cases I through V. Blue dots, orange squares, green diamonds, red upright triangles and purple inverted triangles correspond to the propulsion case I, II, III, IV and V, respectively.

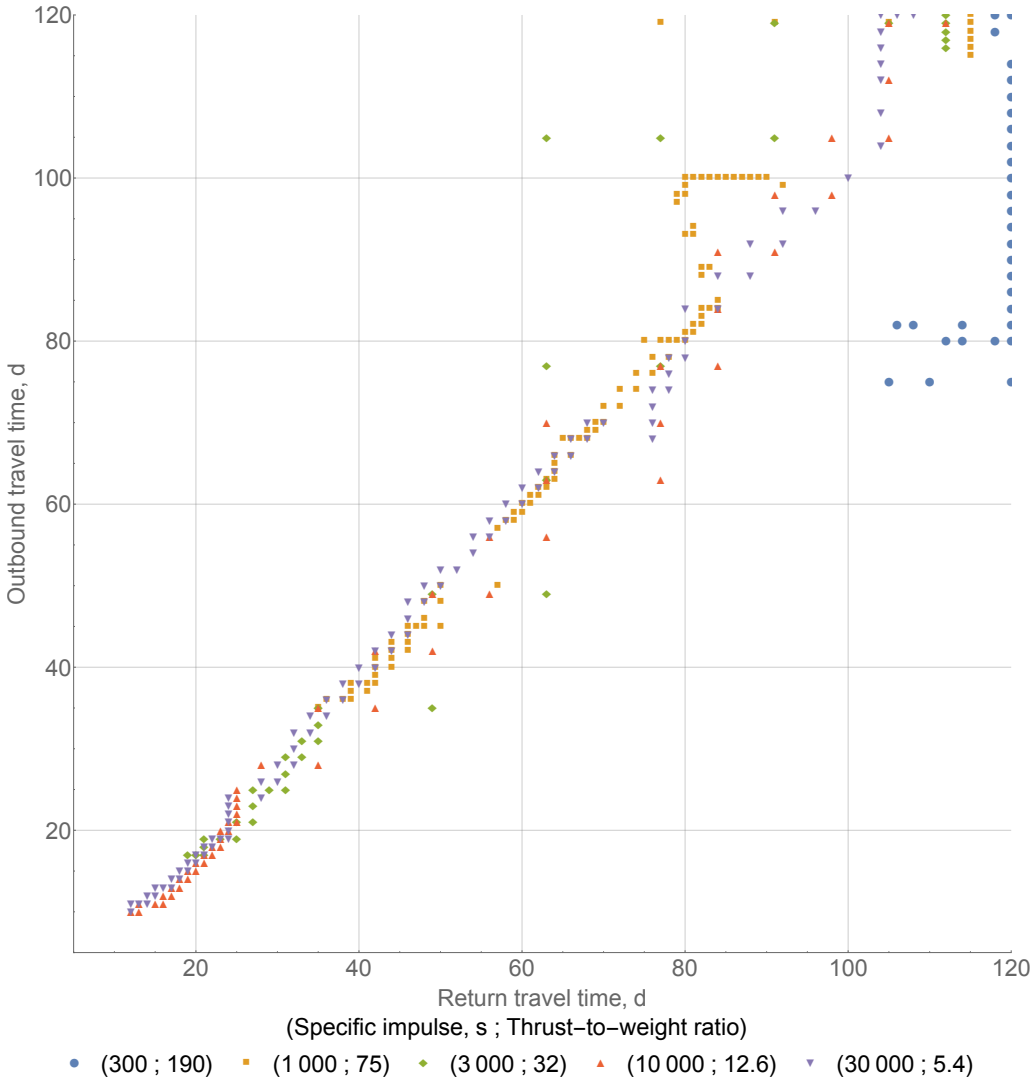

Figure 4.10: Relation between outbound and return travel times for option B and propulsion cases I through V. Blue dots, orange squares, green diamonds, red upright triangles and purple inverted triangles correspond to the propulsion case I, II, III, IV and V, respectively.

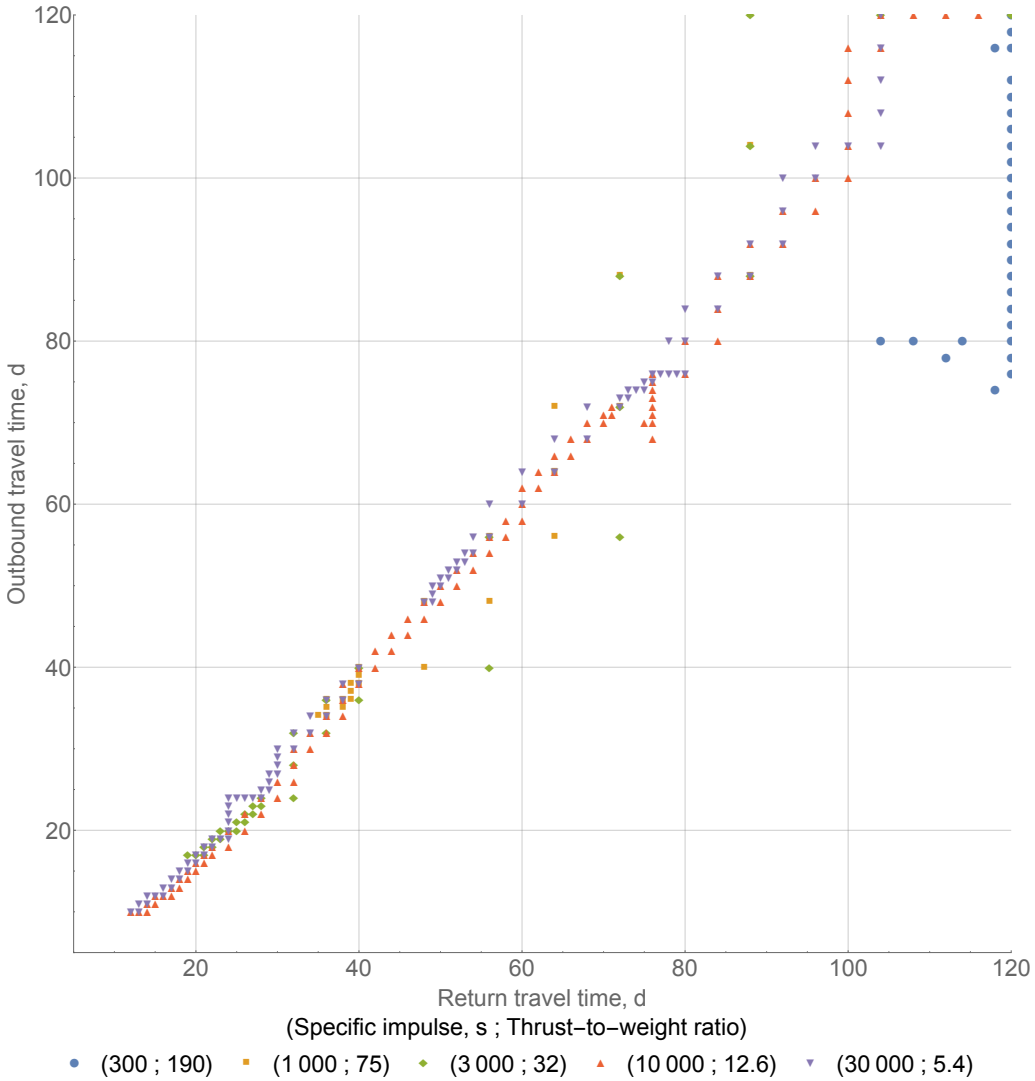

Figure 4.11: Relation between outbound and return travel times for option C and propulsion cases I through V. Blue dots, orange squares, green diamonds, red upright triangles and purple inverted triangles correspond to the propulsion case I, II, III, IV and V, respectively.

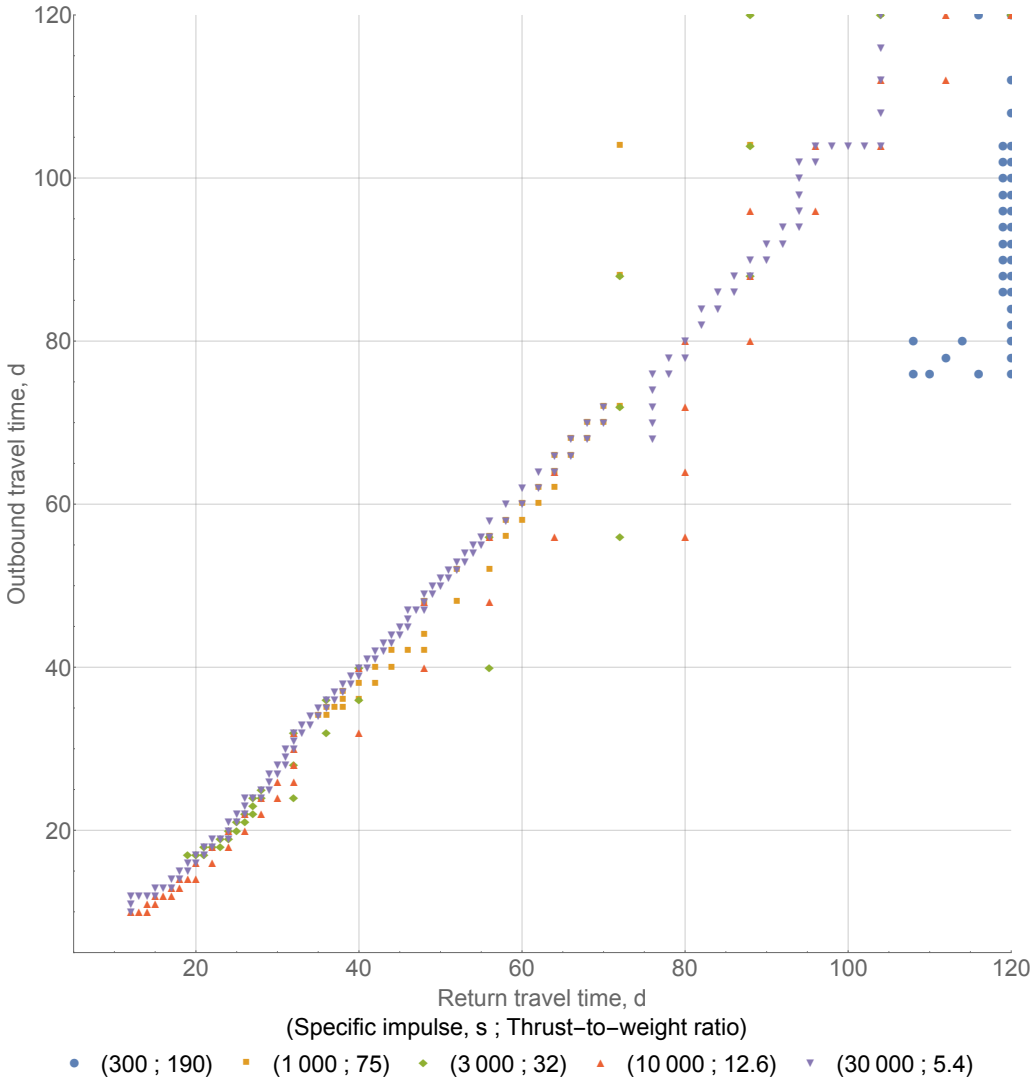

Figure 4.12: Relation between outbound and return travel times for option D and propulsion cases I through V. Blue dots, orange squares, green diamonds, red upright triangles and purple inverted triangles correspond to the propulsion case I, II, III, IV and V, respectively.

Chapter 5

Conclusions

This work determines the trade-off between IMLEO and round trip time for rapid crewed missions to Mars with high-thrust. The most promising architectures were identified, and the required elements estimated. Finally, different characteristic values were selected for both modern and foreseen propulsion systems.

It has been found that there is a minimum value for the travel time, which depends on the characteristics of the propulsion system used. Such limit stems from the inclusion of a burn losses term in the rocket equation. Due to that same term, there is an optimum thrust value that yields the lowest IMLEO for a certain total trip time. This behaviour differs greatly from the traditional rocket equation, for which there is a solution to every total trip time. In the ideal case, the propellant mass increases monotonically with thrust through the propulsion system mass (with higher increases for lower thrust-to-weight ratios).

The large amount of propellant required constitutes most of the mass. For this reason, all considered architectures performed equally for faster missions and showed only small differences for slower ones. In particular, the usage of ISRU for the production of ascent propellant makes no significant difference for rapid trips.

Finally, this work suggests that this type of mission can be possible in the future. For comparison, DRA 5.0 states an IMLEO of about $849\,\mathrm{t}$ for a round trip time of $916\,\mathrm{d}$ [5]. For the same mass, the mission can be achieved in about $200\,\mathrm{d}$ with case II propulsion.

5.1 Future Work

This work is a first approach to address the problem, and was developed at the level of preliminary design. There are subjects in need of development, which require a dedicated approach. Some can be found in the literature, albeit in a non-applicable range for the rapid mission concept. Namely, burn losses estimation, re-entry and aerocapture. Although the last should still be studied, chances are that the mass savings will not be significant enough (due to TPS limitations) in this same context, much like ISRU usage for Mars ascent propellant production. Trajectory-wise, the calculations need to be extended to the real case, with eccentric and non-coplanar orbits.

Of particular importance is whether or not ISRU can be used for the production of the return propel-

lant. This will demand a considerable re-design of the mission in order to solve the problem of transporting the propellant to orbit. But with the vast majority of the IMLEO concentrated in the propellant, there is potential for large savings by producing it on site rather than carrying it from Earth.

References

[1] Wertz, J. R., "Interplanetary Round Trip Mission Design," *Acta Astronautica*, Vol. 55, No. 3, 2004, pp. 221 – 232. https://doi.org/10.1016/j.actaastro.2004.05.019.

[2] Tripathi, R. K., and Nealy, J. E., "Mars Radiation Risk Assessment and Shielding Design for Long-Term Exposure to Ionizing Space Radiation," *2008 IEEE Aerospace Conference*, 2008, pp. 1–9.

[3] Kanas, N., and Manzey, D., *Space Psychology and Psychiatry*, 2nd ed., Space Technology Library, Vol. 22, Springer, 2008. https://doi.org/10.1007/978-1-4020-6770-9.

[4] Amade, N. S., and Wertz, J., "Design of a Mars Rapid Round Trip Mission," *AIAA SPACE 2010 Conference & Exposition*, 2010. https://doi.org/10.2514/6.2010-8642.

[5] Drake, B. G. (ed.), *Human Exploration of Mars Design Reference Architecture 5.0*, NASA-SP-2009-566, 2009.

[6] Salotti, J. M., "New Trade Tree for Manned Mars Missions," *Acta Astronautica*, Vol. 104, No. 2, 2014, pp. 574 – 581. https://doi.org/https://doi.org/10.1016/j.actaastro.2014.07.017.

[7] Salotti, J. M., Heidmann, R., and Suhir, E., "Crew Size Impact on the Design, Risks and Cost of a Human Mission to Mars," *2014 IEEE Aerospace Conference*, 2014, pp. 1–9. https://doi.org/10.1109/AERO.2014.6836241.

[8] Salotti, J. M., and Claverie, B., "Human Mission to Mars: All-up vs Pre-deploy." *Global Space Exploration Conference*, 2012.

[9] Christian, J. A., Wells, G., Lafleur, J. M., Verges, A., and Braun, R. D., "Extension of Traditional Entry, Descent, and Landing Technologies for Human Mars Exploration," *Journal of Spacecraft and Rockets*, Vol. 45, No. 1, 2008, pp. 130–141. https://doi.org/10.2514/1.31929.

[10] Interbartolo, M. A., Sanders, G. B., Oryshchyn, L., Lee, K., Vaccaro, H., Santiago-Maldonado, E., and Muscatello, A. C., "Prototype Development of an Integrated Mars Atmosphere and Soil-Processing System," *Journal of Aerospace Engineering*, Vol. 26, No. 1, 2013, pp. 57–66. https://doi.org/10.1061/(ASCE)AS.1943-5525.0000214.

[11] Kleinhenz, J. E., and Paz, A., "An ISRU Propellant Production System for a Fully Fueled Mars Ascent Vehicle," *10th Symposium on Space Resource Utilization*, 2017. https://doi.org/10.2514/6.2017-0423.

[12] Starr, S. O., and Muscatello, A. C., "Mars In Situ Resource Utilization: A Review," *Planetary and Space Science*, Vol. 182, 2020, p. 104824. https://doi.org/https://doi.org/10.1016/j.pss.2019.104824.

[13] Hughes, K. M., Edelman, P. J., Longuski, J., Loucks, M., Carrico, J. P., and Tito, D. A., "Fast Mars Free-Returns via Venus Gravity Assist," *AIAA/AAS Astrodynamics Specialist Conference*, 2014. https://doi.org/10.2514/6.2014-4109.

[14] Landau, D., and Longuski, J., "A Reassessment of Trajectory Options for Human Missions to Mars," *AIAA/AAS Astrodynamics Specialist Conference and Exhibit*, 2004. https://doi.org/10.2514/6.2004-5095.

[15] Nordley, G. D., and Forward, R. L., "Mars-Earth Rapid Interplanetary Tether Transport System: I. Initial Feasibility Analysis," *Journal of Propulsion and Power*, Vol. 17, No. 3, 2001, pp. 499–507. https://doi.org/10.2514/2.5798.

[16] Guerra, A. G. C., Bertolami, O., and Gil, P. J. S., "Comparison of Four Space Propulsion Methods for Reducing Transfer Times of Manned Mars Mission," https://arxiv.org/abs/1502.06457, 2015.

[17] Zubrin, R., *The Case for Mars*, 1st ed., Simon & Schuster, 2011.

[18] Tito, D. A., Anderson, G., Carrico, J. P., Clark, J., Finger, B., Lantz, G. A., Loucks, M. E., MacCallum, T., Poynter, J., Squire, T. H., and Worden, S. P., "Feasibility Analysis for a Manned Mars Free-Return Mission in 2018," *2013 IEEE Aerospace Conference*, 2013, pp. 1–18. https://doi.org/10.1109/AERO.2013.6497413.

[19] Spilker, T. R., Adler, M., Arora, N., Beauchamp, P. M., Cutts, J. A., Munk, M. M., Powell, R. W., Braun, R. D., and Wercinski, P. F., "Qualitative Assessment of Aerocapture and Applications to Future Missions," *Journal of Spacecraft and Rockets*, Vol. 56, No. 2, 2019, pp. 536–545. https://doi.org/10.2514/1.A34056.

[20] Drake, B. G. (ed.), *Human Exploration of Mars Design Reference Architecture 5.0 Addendum*, NASA/SP-2009-566-ADD, 2009.

[21] Young, J. W., and Smith, Jr., R. E., "Trajectory Optimization for an Apollo-Type Vehicle Under Entry Conditions Encountered During Lunar Return," Technical Report NASA-TR-R-258, NASA, May 1967.

[22] Ward, E. D., Webb, R. R., and deWeck, O. L., "A Method to Evaluate Utility for Architectural Comparisons for a Campaign to Explore the Surface of Mars," *Acta Astronautica*, Vol. 128, 2016, pp. 237 – 242. https://doi.org/https://doi.org/10.1016/j.actaastro.2016.07.022.

[23] Salotti, J. M., "Human Mission to Mars: The 2-4-2 Concept," Technical Report 2012-5-242, Institut Polytechnique de Bordeaux, May 2011.

[24] Putnam, Z. R., Braun, R. D., Rohrschneider, R. R., and Dec, J. A., "Entry System Options for Human Return from the Moon and Mars," *Journal of Spacecraft and Rockets*, Vol. 44, No. 1, 2007, pp. 194–202. https://doi.org/10.2514/1.20351.

[25] Jones, H. W., "Would Current International Space Station (ISS) Recycling Life Support Systems Save Mass on a Mars Transit?" *47th International Conference on Environmental Systems*, 2017.

[26] "Human Integration Desing Handbook," Special Publication NASA/SP-2010-3407/REV1, NASA, January 2014.

[27] Anderson, M. S., Ewert, M. K., and Keener, J. F., "Life Support Baseline Values and Assumptions Document," Technical Publication NASA/TP-2015-218570/REV1, NASA, January 2018.

[28] Boden, R. C., "Mass Estimation Tool for Human Space Missions," Master's thesis, Technische Universität München, 2013.

[29] Sforza, P. M., *Manned Spacecraft Design Principles*, Elsevier, 2016.

[30] Polsgrove, T. P., Percy, T. K., Rucker, M., and Thomas, H. D., "Update to Mars Ascent Vehicle Design for Human Exploration," *2019 IEEE Aerospace Conference*, 2019, pp. 1–15. https://doi.org/10.1109/AERO.2019.8741709.

[31] Drake, B. G., and Watts, K. D. (eds.), *Human Exploration of Mars Design Reference Architecture 5.0 Addendum #2*, NASA/SP-2009-566-ADD2, 2014.

[32] Polsgrove, T., Thomas, H. D., Sutherlin, S., Stephens, W., and Rucker, M. A., "Mars Ascent Vehicle Design for Human Exploration," *AIAA SPACE 2015 Conference and Exposition*, 2015. https://doi.org/10.2514/6.2015-4416.

[33] Laub, B., and Venkatapathy, E., "Thermal Protection System Technology and Facility Needs for Demanding Future Planetary Missions," *Planetary Probe Atmospheric Entry and Descent Trajectory Analysis and Science*, ESA Special Publication, Vol. 544, edited by A. Wilson, 2004, pp. 239–247.

[34] Chapman, D. R., "An Approximate Analytical Method for Studying Entry into Planetary Atmospheres," Technical Note NACA-TN-4276, NASA, May 1958.

[35] Tauber, M. E., and Sutton, K., "Stagnation-Point Radiative Heating Relations for Earth and Mars Entries," *Journal of Spacecraft and Rockets*, Vol. 28, No. 1, 1991, pp. 40–42. https://doi.org/10.2514/3.26206.

[36] Wiesel, W. E., *Spaceflight Dynamics*, 3rd ed., Aphelion Press, 2010.

[37] Robbins, H. M., "An Analytical Study of the Impulsive Approximation," *AIAA Journal*, Vol. 4, No. 8, 1966, pp. 1417–1423. https://doi.org/10.2514/3.3687.

[38] Confraria, J. C. F., "Finite Burn Losses in Spacecraft Maneuvres Revisited," Master's thesis, Instituto Superior Técnico, 2020.

[39] Cassenti, B. N., "Trajectory Options for Manned Mars Missions," *Journal of Spacecraft and Rockets*, Vol. 42, No. 5, 2005, pp. 890–895. https://doi.org/10.2514/1.9770.

[40] Lang, S., *Complex Analysis*, 4th ed., Graduate Texts in Mathematics, Vol. 103, Springer-Verlag New York, 1999. https://doi.org/10.1007/978-1-4757-3083-8.

[41] da Silva Rodrigues Pinto, J. T., "A Survey of Modern and Future Space Propulsion Methods," Master's thesis, Instituto Superior Técnico, 2019.

[42] Ding, Y., and Shen, Z., "Investigation of the Radiation Environment in Deep Space and Its Effect on Spacecraft Materials Properties," *Protection of Materials and Structures from the Space Environment*, edited by J. Kleiman, Springer International Publishing, Cham, 2017, pp. 471–479.

[43] Walberg, G., "How shall we go to Mars? A review of mission scenarios," *Journal of Spacecraft and Rockets*, Vol. 30, No. 2, 1993, pp. 129–139. https://doi.org/10.2514/3.11521.

[44] Hartvigsen, J., Elangovan, S., Elwell, J., and Larsen, D., "Oxygen Production from Mars Atmosphere Carbon Dioxide Using Solid Oxide Electrolysis," *ECS Transactions*, Vol. 78, No. 1, 2017, pp. 2953–2963. https://doi.org/10.1149/07801.2953ecst.

[45] Hall, J. L., Noca, M. A., and Bailey, R. W., "Cost-Benefit Analysis of the Aerocapture Mission Set," *Journal of Spacecraft and Rockets*, Vol. 42, No. 2, 2005, pp. 309–320. https://doi.org/10.2514/1.4118.

[46] Machado, L. B., and Wilde, M., "Parametric Design of a Crew Transfer Vehicle for Earth–Mars Cyclers," *Journal of Spacecraft and Rockets*, Vol. 57, No. 3, 2020, pp. 565–579. https://doi.org/10.2514/1.A34637.